CERN-PH-EP/2012-202
2013/01/29

CMS-FSQ-12-014

Study of the inclusive production of charged pions, kaons, and protons in pp collisions at $\sqrt{s} = 0.9, 2.76, \text{ and } 7 \text{ TeV}$

The CMS Collaboration*

Abstract

Spectra of identified charged hadrons are measured in pp collisions at the LHC for $\sqrt{s} = 0.9, 2.76, \text{ and } 7 \text{ TeV}$. Charged pions, kaons, and protons in the transverse-momentum range $p_T \approx 0.1\text{--}1.7 \text{ GeV}/c$ and for rapidities $|y| < 1$ are identified via their energy loss in the CMS silicon tracker. The average p_T increases rapidly with the mass of the hadron and the event charged-particle multiplicity, independently of the center-of-mass energy. The fully corrected p_T spectra and integrated yields are compared to various tunes of the PYTHIA 6 and PYTHIA 8 event generators.

Submitted to the European Physical Journal C

*See Appendix A for the list of collaboration members

1 Introduction

The study of hadron production has a long history in high-energy particle and nuclear physics, as well as cosmic-ray physics. The absolute yields and the transverse momentum (p_T) spectra of identified hadrons in high-energy hadron-hadron collisions are among the basic physical observables that can be used to test the predictions for non-perturbative quantum chromodynamics processes like hadronization and soft parton interactions, and their implementation in Monte Carlo (MC) event generators. The dependence of these quantities on the hardness of the pp collision provides valuable information on multi-parton interactions as well as on other final-state effects. In addition, the measurements of baryon (and notably proton) production are not reproduced by the existing models, and more data at higher energy may help improving the models. Spectra of identified particles in proton-proton (pp) collisions also constitute an important reference for high-energy heavy-ion studies, where final-state effects are known to modify the spectral shape and yields of different hadron species.

The present analysis focuses on the measurement of the p_T spectra of charged hadrons, identified mostly via their energy deposits in silicon detectors, in pp collisions at $\sqrt{s} = 0.9, 2.76$, and 7 TeV. In certain phase space regions, particles can be identified unambiguously while in other regions the energy loss measurements provide less discrimination power and more sophisticated methods are necessary.

This paper is organized as follows. The Compact Muon Solenoid (CMS) detector, operating at the Large Hadron Collider (LHC), is described in Section 2. Elements of the data analysis, such as event selection, tracking of charged particles, identification of interaction vertices, and treatment of secondary particles are discussed in Section 3. The applied energy loss parametrization, the estimation of energy deposits in the silicon, and the calculation of the energy loss rate of tracks are explained in Section 4. In Section 5 the various aspects of the unfolding of particle yields are described. After a detailed discussion of the applied corrections (Section 6), the final results are shown in Section 7 and summarized in the conclusions.

2 The CMS detector

The central feature of the CMS apparatus is a superconducting solenoid of 6 m internal diameter. Within the field volume are the silicon pixel and strip tracker, the crystal electromagnetic calorimeter, and the brass/scintillator hadron calorimeter. In addition to the barrel and endcap detectors, CMS has extensive forward calorimetry. CMS uses a right-handed coordinate system, with the origin at the nominal interaction point and the z axis along the counterclockwise beam direction. The pseudorapidity and rapidity of a particle with energy E , momentum p , and momentum along the z axis p_z are defined as $\eta = -\ln \tan(\theta/2)$ where θ is the polar angle with respect to the z axis and $y = \frac{1}{2} \ln[(E + p_z)/(E - p_z)]$, respectively. A more detailed description of CMS can be found in Ref. [1].

Two elements of the CMS detector monitoring system, the beam scintillator counters (BSCs) and the beam pick-up timing for the experiments (BPTX) devices, were used to trigger the detector readout. The two BSCs are located at a distance of ± 10.86 m from the nominal interaction point (IP) and are sensitive to particles in the $|\eta|$ range from 3.23 to 4.65. Each BSC is a set of 16 scintillator tiles. The BSC elements are designed to provide hit and coincidence rates. The two BPTX devices, located around the beam pipe at a distance of 175 m from the IP on either side, are designed to provide precise information on the bunch structure and timing of the incoming beam. A steel/quartz-fibre forward calorimeter (HF) covers the region of $|\eta|$ between about 3.0 and 5.0. The HF tower segmentation in η and azimuthal angle ϕ is 0.175×0.175 , except for $|\eta|$

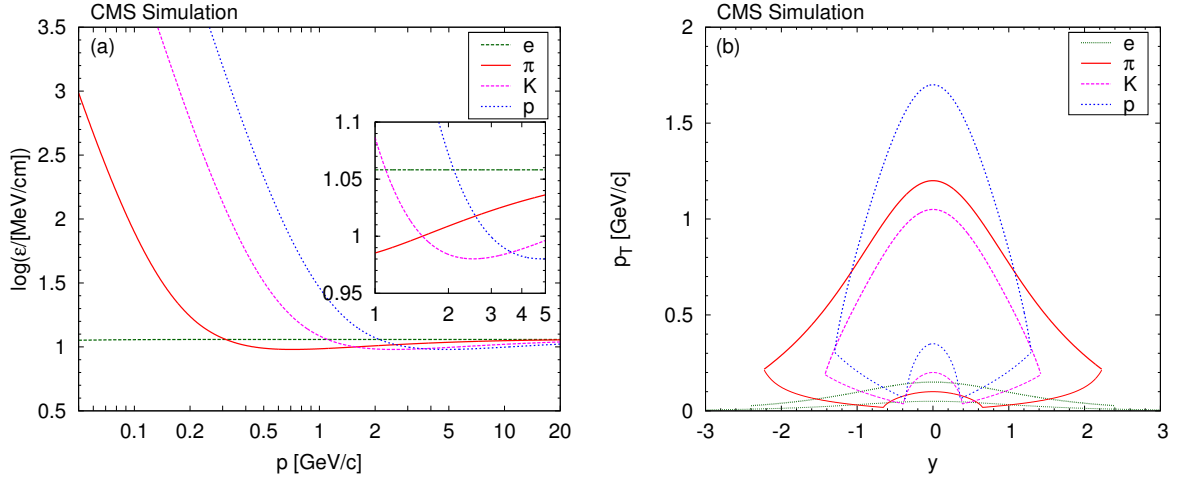


Figure 1: **(a)** Values of the most probable energy loss rate ϵ , at the reference path length of $450 \mu\text{m}$ in silicon, for electrons, pions, kaons and protons [2]. The inset shows the region $1 < p < 5 \text{ GeV}/c$. **(b)** For each particle, the accessible (y, p_T) area is contained between the upper thicker (determined by particle identification capabilities) and the lower thinner lines (determined by acceptance and efficiency). More details are given in Section 2.1.

above 4.7 where the segmentation is 0.175×0.35 .

The tracker measures charged particles within the pseudorapidity range $|\eta| < 2.4$. It has 1440 silicon pixel and 15148 silicon strip detector modules and is located in the 3.8 T field of the solenoid. The pixel detector [3] consists of three barrel layers (PXB) at radii of 4.4, 7.3, and 10.2 cm as well as two endcap disks (PXF) on each side of the PXB. The detector units are segmented n-on-n silicon sensors of $285 \mu\text{m}$ thickness. Each readout chip serves a 52×80 array of $150 \mu\text{m} \times 100 \mu\text{m}$ pixels. In the data acquisition system, zero suppression is performed with adjustable thresholds for each pixel. Offline, pixel clusters are formed from adjacent pixels, including both side-by-side and corner-by-corner adjacent pixels. The strip tracker [4] employs p-in-n silicon wafers. It is partitioned into different substructures: the tracker inner barrel (TIB) and the tracker inner disks (TID) are the innermost part with $320 \mu\text{m}$ thick sensors, surrounded by the tracker outer barrel (TOB) with $500 \mu\text{m}$ thick sensors. On both sides, the tracker is completed by endcaps with a mixture of $320 \mu\text{m}$ thick sensors (TEC3) and $500 \mu\text{m}$ thick sensors (TEC5). The first two layers of TIB and TOB and some of the TID and TEC contain “stereo” modules: two silicon modules mounted back-to-back with a 100 mrad angle to provide two-dimensional hit resolution. Each readout chip serves 128 strips. Algorithms are run in the Front-End Drivers (FED) to perform pedestal subtraction, common-mode subtraction and zero suppression. Only a small fraction of the channels are read out in one event. Offline, clusters are formed by combining contiguous hits. The tracker provides an impact-parameter resolution of $\sim 15 \mu\text{m}$ and an absolute p_T resolution of about $0.02 \text{ GeV}/c$ in the range $p_T \approx 0.1\text{--}2 \text{ GeV}/c$, of relevance here.

2.1 Particle identification capabilities

The identification of charged particles is often based on the relationship between energy loss rate and total momentum (Fig. 1a). Particle reconstruction at CMS is limited by the acceptance (C_a) of the tracker ($|\eta| < 2.4$) and by the low tracking efficiency (C_e) at low momentum ($p > 0.05, 0.10, 0.20$, and $0.35 \text{ GeV}/c$ for e, π , K, and p, respectively), while particle identification capabilities are restricted to $p < 0.15 \text{ GeV}/c$ for electrons, $p < 1.20 \text{ GeV}/c$ for pions,

$p < 1.05 \text{ GeV}/c$ for kaons, and $p < 1.70 \text{ GeV}/c$ for protons (Fig. 1a). Pions are accessible up to a higher momentum than kaons because of their high relative abundance, as discussed in Section 5.2. The (y, p_T) region where pions, kaons and protons can all be identified is visible in Fig. 1b. The region $-1 < y < 1$ was chosen for the measurement, since it maximizes the p_T coverage.

3 Data analysis

The 0.9 and 7 TeV data were taken during the initial low multiple-interaction rate (low “pileup”) runs in early 2010, while the 2.76 TeV data were collected in early 2011. The requirement of similar amounts of produced particles at the three center-of-mass energies and that of small average number of pileup interactions led to 8.80, 6.74 and 6.20 million events for $\sqrt{s} = 0.9 \text{ TeV}$, 2.76 TeV, and 7 TeV, respectively. The corresponding integrated luminosities are $0.227 \pm 0.024 \text{ nb}^{-1}$, $0.143 \pm 0.008 \text{ nb}^{-1}$ and $0.115 \pm 0.005 \text{ nb}^{-1}$ [5, 6], respectively.

3.1 Event selection and related corrections

The event selection consists of the following requirements:

- at the trigger level, the coincidence of signals from both BPTX devices, indicating the presence of both proton bunches crossing the interaction point, along with the presence of signals from either of the BSCs;
- offline, the presence of at least one tower with energy above 3 GeV in each of the HF calorimeters; at least one reconstructed interaction vertex (Section 3.3); the suppression of beam-halo and beam-induced background events, which usually produce an anomalously large number of pixel hits [7].

The efficiencies for event selection, tracking, and vertexing were evaluated by means of simulated event samples produced with the PYTHIA 6.420 [8] MC event generator at each of the three center-of-mass energies. The events were reconstructed in the same way as the collision data. The PYTHIA tunes D6T [9], Z1, and Z2 [10] were chosen, since they describe the measured event properties reasonably well, notably the reconstructed track multiplicity distribution. Tune D6T is a pre-LHC tune with virtuality-ordered showers using the CTEQ6L parton distribution functions (PDF). The tunes Z1 and Z2 are based on the early LHC data and generate p_T -ordered showers using the CTEQ5L and CTEQ6L PDFs, respectively.

The final results were corrected to a particle level selection, which is very similar to the actual selection described above: at least one particle ($\tau > 10^{-18} \text{ s}$) with $E > 3 \text{ GeV}$ in the range $-5 < \eta < -3$ and one in the range $3 < \eta < 5$; this selection is referred to in the following as “double-sided” (DS) selection. The overall efficiency of the DS selection for a zero-bias sample, according to PYTHIA, is about 66-72% (0.9 TeV), 70-76% (2.76 TeV), and 73-78% (7 TeV). The ranges given represent the spread of the predictions of the different tunes. Mostly non-diffractive (ND) events are selected, with efficiencies in the 88-98% range, but a smaller fraction of double-diffractive (DD) events (32-38%), and single-diffractive dissociation (SD) events are accepted (13-26%) as well. About 90% of the selected events are ND, while the rest are DD or SD, in about equal measure. In order to compare to measurements with a non-single-diffractive (NSD) selection, the particle yields given in this study should be divided by factors of 0.86, 0.89, and 0.91 according to PYTHIA, for $\sqrt{s} = 0.9, 2.76$, and 7 TeV, respectively. The systematic uncertainty on these numbers due to the tune dependence is about 3%.

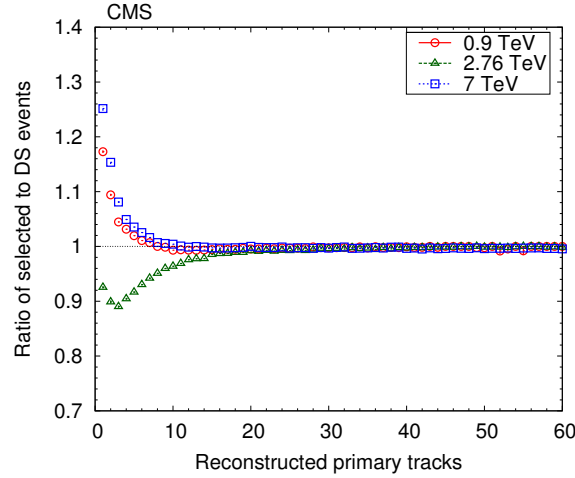


Figure 2: The ratio of selected events to double-sided events (ratio of the corresponding efficiencies in the inelastic sample), according to the PYTHIA6 tunes (0.9 TeV– D6T, 2.76 TeV– Z2, 7 TeV– Z1), as a function of the reconstructed primary charged track multiplicity.

The ratios of the data selection efficiency to the DS selection efficiency are shown as a function of the reconstructed track multiplicity in Fig. 2 for the three center-of-mass energies studied. The ratios are used to correct the measured events; they are approximately independent of the PYTHIA tune. The different behavior of the 2.76 TeV data results from a change in the HF configuration in 2011. The results are also corrected for the fraction of DS events without a reconstructed track. This fraction, as given by the simulation, is about 4%, 3%, and 2.5% for 0.9, 2.76, and 7 TeV, respectively. Since these events do not contain reconstructed tracks, only the event yield must be corrected.

3.2 Tracking of charged particles

The extrapolation of particle spectra into the unmeasured regions is model dependent, particularly at low p_T . A good measurement therefore requires reliable track reconstruction down to the lowest possible p_T . The present analysis extends to $p_T \approx 0.1 \text{ GeV}/c$ by exploiting special tracking algorithms [11], used in previous studies [7, 12], to provide high reconstruction efficiency and low background rate. The charged pion hypothesis was assumed when fitting particle momenta.

The performance of the charged-particle tracking was quantified in terms of the geometrical acceptance, the tracking efficiency, and the fraction of misreconstructed tracks; all these quantities were evaluated by means of simulated events and validated in previous studies [7, 12]. The acceptance of the tracker (when at least two pixel hits are required) is flat in the region $-2 < \eta < 2$ and $p_T > 0.4 \text{ GeV}/c$, and its value is about 96–98%. The loss of acceptance at $p_T < 0.4 \text{ GeV}/c$ is caused by energy loss and multiple scattering of particles, which both depend on the particle mass. Likewise, the reconstruction efficiency is about 80–90%, degrading at low p_T , also in a mass-dependent way. The misreconstructed-track rate (C_f) is very small, reaching 0.3% only for $p_T < 0.25 \text{ GeV}/c$; it rises slightly above 2 GeV/c because of the steeply falling p_T distribution. The probability of reconstructing multiple tracks (C_m) from a true single track is about 0.1% – mostly due to particles spiralling in the strong magnetic field. The efficiencies and background rates largely factorize in η and p_T , but for the final corrections an (η, p_T) grid is used.

Table 1: Standard deviation of the vertex z coordinate distribution (σ_z) and average number of pileup events for the three center-of-mass energies studied. The last two columns show the estimated fraction of merged and split vertices. More details are given in the text.

<i>Energy</i>	σ_z	$\langle \text{pileup} \rangle$	<i>Merged</i>	<i>Split</i>
0.9 TeV	6.67 cm	0.016	$5 \cdot 10^{-4}$	$\sim 10^{-3}$
2.76 TeV	6.23 cm	0.094	$3 \cdot 10^{-3}$	$\sim 10^{-3}$
7 TeV	3.08 cm	0.009	$6 \cdot 10^{-4}$	$\sim 10^{-3}$

3.3 Vertexing and secondary particles

The region where pp collisions occur (beam spot) is well measured by reconstructing vertices from many events. Since the bunches are very narrow, the transverse position of the interaction vertices is well constrained; conversely, their z coordinates are spread over a relatively long distance and must be determined on an event-by-event basis. Reconstructed tracks are used for determining the vertex position if they have $p_T > 0.1$ GeV/ c and originate from the vicinity of the beam spot, i.e. their transverse impact parameter satisfies the condition $d_T < 3\sigma_T$; here σ_T is the quadratic sum of the uncertainty of d_T and the RMS of the beam spot distribution in the transverse plane. The agglomerative vertex-reconstruction algorithm [13] was used, with the z coordinates (and their uncertainty) of the tracks at the point of closest approach to the beam axis as input. This algorithm keeps clustering tracks into vertices as long as the smallest distance between the vertices of the remaining groups of tracks, divided by its uncertainty, is below 35. Simulations indicate that this value minimizes the number of merged vertices (vertices with tracks from two or more true vertices) and split vertices (two or more vertices with tracks from a single true vertex). For single-vertex events, there is no lower limit on the number of tracks associated to the vertex. If multiple vertices are present, only those with at least three tracks are kept.

The distribution of the z coordinates of the reconstructed primary vertices is Gaussian, with standard deviations of 6 cm at 0.9 and 2.76 TeV, and 3 cm at 7 TeV. The simulated data were reweighted so as to have the same vertex z coordinate distributions as the data. The distribution of the distance Δz between vertices was used to quantify the effect of pileup and the quality of vertex reconstruction. There is an empty region around $\Delta z = 0$, which corresponds to cases in which two true vertices are closer than about 0.4 cm to each other and are merged during vertex reconstruction. The Δz distribution was therefore used to determine the fraction of merged (and thus lost) vertices, and to estimate the fraction of split vertices (via the non-Gaussian tails). Both effects are at the 0.1% level and were neglected in this study.

The number of primary vertices in a bunch crossing follows a Poisson distribution. The fraction of events with more than one vertex (due to pileup) is small in the 0.9 and 7 TeV data (1.6% and 0.9%, respectively), but is 9.4% at 2.76 TeV. The interaction-region and pileup parameters are summarized in Table 1. For the 0.9 and 2.76 TeV data, bunch crossings with either one or two reconstructed vertices were used, while for the 7 TeV data the analysis was restricted to events with a single reconstructed vertex to suppress the larger background from pileup, split and merged vertices.

The hadron spectra were corrected for particles of non-primary origin. The main source of secondary particles is the feed-down from weakly decaying particles, mostly K_S^0 , $\Lambda/\bar{\Lambda}$, and $\Sigma^+/\bar{\Sigma}^-$. While the correction (C_s) is around 1% for pions, it is up to 15% for protons with $p_T \approx 0.2$ GeV/ c . This is expected because the daughter p or \bar{p} takes most of the momentum of the

Table 2: Properties of several strip subdetectors evaluated by using hits on tracks with close-to-normal incidence: readout threshold t , coupling parameter α_c , standard deviation σ_n of the Gaussian noise. The three values given for α_c and σ_n are for the 0.9, 2.76, and 7 TeV datasets.

Detector	t [keV]	α_c	σ_n [keV]
TIB	9.6	0.091, 0.077, 0.096	6.9, 7.0, 6.9
TID	8.5	0.076, 0.068, 0.081	7.2, 7.6, 7.2
TOB	15.3	0.116, 0.094, 0.124	9.2, 10.3, 9.6
TEC3	8.5	0.059, 0.059, 0.072	6.3, 6.9, 6.4
TEC5	14.1	0.094, 0.086, 0.120	8.6, 9.7, 9.0

primary $\Lambda/\bar{\Lambda}$, and therefore has a higher probability of being (mistakenly) fitted to the primary vertex than a pion from a K_S^0 decay. Since none of the weakly decaying particles mentioned decay into kaons, the correction for kaons is small. The corrections were derived from PYTHIA and cross-checked with data [14] by comparing measured and predicted spectra of particles. While data and simulation generally agree, the $\Lambda/\bar{\Lambda}$ correction had to be multiplied by a factor of 1.6.

For $p < 0.15 \text{ GeV}/c$, electrons can be clearly identified. According to PYTHIA, the overall e^\pm contamination of the hadron yields is below 0.2%. Although muons cannot be separated from pions, their fraction is negligible, below 0.05%. Since both contaminations are small no corrections were applied.

4 Energy deposits and estimation of energy loss rate

The silicon layers of the tracker are thin and the energy depositions do not follow a Gaussian distribution, but exhibit a long tail at high values. Ideally, the estimates of the energy loss rate should not depend on the path lengths of the track through the sensitive parts of the silicon or on the detector details. However this is not the case with the often used truncated, power, or weighted means of the differential deposits, $\Delta E/\Delta x$. Some of the dependence on the path length can be corrected for, but a method based on the proper knowledge of the underlying physical processes is preferable.

In the present paper a novel analytical parametrization [15] has been used to approximate the energy loss of charged particles. The method provides the probability density $p(y|\varepsilon, l)$ of energy deposit y , if the most probable energy loss rate ε at a reference path-length l_0 and the path-length l are known. The method can be used in conjunction with a maximum likelihood estimation. The deposited energy is estimated from the measured charge deposits in individual channels (pixels or strips) contributing to hit clusters. Deposits below the readout threshold or above the saturation level of the readout electronics are estimated from the length of the track segment in the silicon. This results in a wider accessible energy deposit range and better particle identification power. The method can be applied to the energy loss rate estimation of tracks and to calibrate the gain of the tracker detector front-end electronics. In this analysis, for each track, the estimated ε value at $l_0 = 450 \mu\text{m}$ was used for particle identification and yield determination.

For pixel clusters, the energy deposits (and their variances) were calculated as the sum of individual pixel deposits (and variances). The noise contribution is Gaussian, with a standard deviation $\sigma_n \approx 10 \text{ keV}$ per pixel. In the case of strips, the energy deposits were corrected for

capacitive coupling and cross-talk between neighboring strips. The readout threshold t , the coupling parameter α_c , and the standard deviation σ_n of the Gaussian noise for strips were determined from the data, by means of tracks with close-to-normal incidence (Table 2).

Table 3: Tight requirements for approximate particle identification. All ε values are functions of p . Subscripts π , K, and p refer to the most probable value for a given particle species, as expected from simulation.

<i>Particle</i>	<i>Momentum</i>	<i>Most probable energy loss rate</i>
pion	$0.15 < p < 0.70 \text{ GeV}/c$	$\varepsilon < (\varepsilon_\pi + \varepsilon_K)/2$
kaon	$p < 0.70 \text{ GeV}/c$	$(\varepsilon_\pi + \varepsilon_K)/2 < \varepsilon < (\varepsilon_K + \varepsilon_p)/2$
proton	$p < 1.40 \text{ GeV}/c$	$(\varepsilon_K + \varepsilon_p)/2 < \varepsilon$

4.1 Detector gain calibration with tracks

For an accurate determination of ε , it is crucial to calibrate the response of all readout chips. It is also important to compare the measured energy deposit spectra to the energy loss parametrization, and introduce corrections if needed.

The value of ε was estimated for each track using an initial gain calibration of the pixel and strip readout chips. Approximate particle identification was performed starting from a sample of identified tracks selected as follows: a track was identified as pion, kaon, or proton if its momentum p and most probable energy loss rate ε satisfied the tight requirements listed in Table 3. In addition, tracks with $p > 2 \text{ GeV}/c$, or $\varepsilon < 3.2 \text{ MeV}/\text{cm}$, or from identified K_S^0 two-body charged decays were assumed to be pions. Identified electrons were not used. The expected ε , path length l , and energy deposit y were collected for each hit, and stored for every readout chip separately. For each chip, the joint energy deposit log-likelihood, $-2 \sum_j \log p(g \cdot y_j | \varepsilon_j, l_j)$, of all selected hits (index j) was minimized by varying the multiplicative gain correction g . At each center-of-mass energy, approximately 10% of the data were sufficient to perform a gain calibration with sufficient resolution. The expected gain uncertainty is 0.5% on average for pixel chips and 0.5-2% for strips readout chips, depending on the chip position.

After the detector gain calibration, the energy loss parametrization was validated with particles identified by the selection discussed above. As examples, the measured energy deposit distributions of positively charged hadrons for different path lengths at $\beta\gamma = p/m = 1.39$ and 3.49 are shown for PXB and TIB in Fig. 3, for the 7 TeV dataset. Similar results were obtained from the data taken at 0.9 and 2.76 TeV. Separate corrections for positive and negative particles were necessary since some effects are not charge symmetric. The energy loss parametrization [15] (solid lines in the figures) gives a good description of the data. In order to describe deviations from the parametrization, we allow for an affine transformation of the theoretical distributions ($\log \varepsilon \rightarrow \alpha \log \varepsilon + \delta$), the parameters of which are determined from the hit-level residuals. The scale factors (α) and the shifts (δ) are both functions of the $\beta\gamma$ value of the particle and the length of the track segment l in silicon. The scale factors are around unity for most $\beta\gamma$ values and increase to 1.2-1.4 for $\beta\gamma < 2$. Shifts (δ) are generally a few keV with deviations up to 10 keV for $\beta\gamma < 1$. A slight path-length dependence was found for both scale factors and shifts. The observed behavior of these hit-level residuals, as a function of $\beta\gamma$ and l , was parametrized with polynomials. These corrections were applied to individual hits during the determination of the $\log \varepsilon$ templates, as described below.

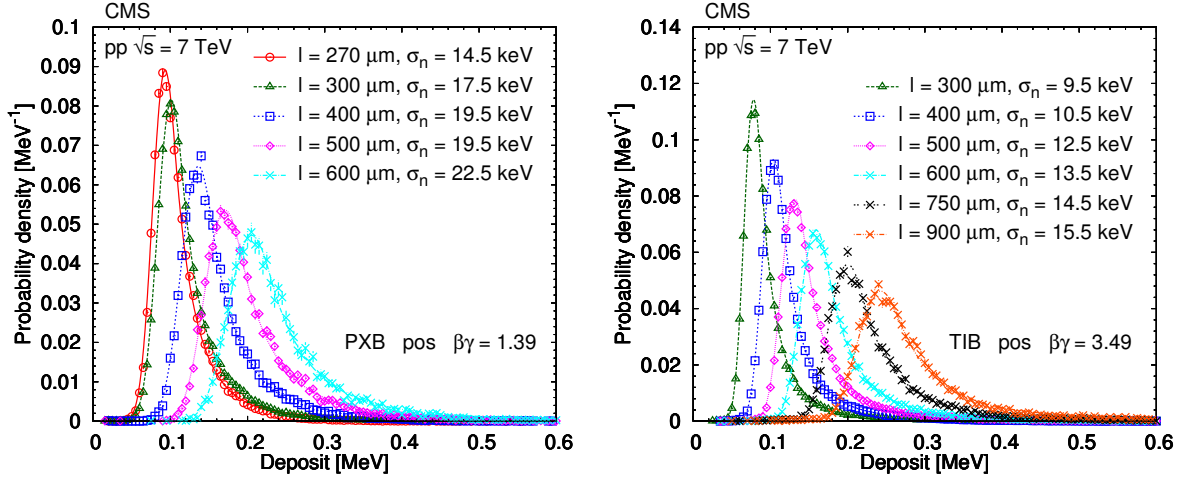


Figure 3: An example from the 7 TeV dataset of the validation of the energy deposit parametrization. The measured energy deposit distributions of identified hadrons at given $\beta\gamma$ values in the PXB (left) and TIB (right) are shown. Values are given for silicon path lengths of $l = 270, 300, 450, 600, 750$, and $900 \mu\text{m}$, together with predictions of the parametrization (curves) already containing the hit-level corrections (scale factors and shifts). The average cluster noise σ_n is also given.

4.2 Estimation of the most probable energy loss rate for tracks

The best value of ε for each track was calculated with the corrected energy deposits. The $\log \varepsilon$ values in (η, p_T) bins were then used in the yield unfolding (Section 5). Removal of hits with incompatible energy deposits and the creation of fit templates, giving the expected $\log \varepsilon$ distributions for all particle species (electrons, pions, kaons, and protons), are discussed here.

The value of ε was estimated by minimizing the joint energy deposit negative log-likelihood of all hits on the trajectory (index i), $\chi^2 = -2 \sum_i \log p(y_i | \varepsilon, l_i)$. Distributions of $\log \varepsilon$ as a function of total momentum p are plotted in Fig. 4 for electrons, pions, kaons, and protons, and compared to the predictions of the energy loss method. The low momentum region is not well described, with the $\log \varepsilon$ estimates slightly shifted towards higher values. This is because charged particles slow down when traversing the detector, which leads to hits with higher average energy deposit than expected by the parameterization. The observed deviations were taken into account by means of track-level corrections (cf. Section 5).

Since the association of hits to tracks is not always unambiguous, some hits, usually from noise or hit overlap, do not belong to the actual track. These false hits, or “outliers”, can be removed. The tracks considered for hit removal were those with at least three hits and for which the joint energy-deposit χ^2 is larger than $1.3 n_{\text{hits}} + 4\sqrt{1.3 n_{\text{hits}}}$, where n_{hits} denotes the number of hits on the track. If the exclusion of a hit decreased the χ^2 by at least 12, the hit was removed. At most one hit was removed; this affected about 1.5% of the tracks. If there is an outlier, it is usually the hit with the lowest $\Delta E / \Delta x$ value.

In addition to the most probable value of $\log \varepsilon$, the shape of the $\log \varepsilon$ distribution was also determined from the data. The template distribution for a given particle species was built from tracks with estimated ε values within three standard deviations of the theoretical value at a given $\beta\gamma$. All kinematical parameters and hit-related observables were kept, but the energy deposits were re-generated by sampling from the analytical parametrization. This procedure exploits the success of the method at the hit level to ensure a meaningful template determina-

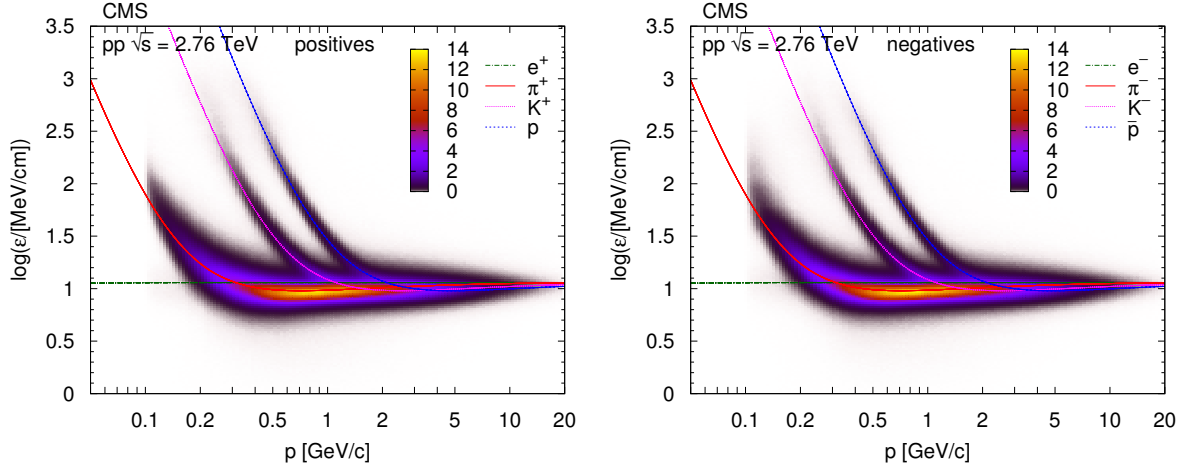


Figure 4: Distribution of $\log \varepsilon$ values as a function of total momentum p for the 2.76 TeV dataset, for positive (left) and negative particles (right). The z scale is shown in arbitrary units and is linear. The curves show the expected $\log \varepsilon$ for electrons, pions, kaons, and protons [2].

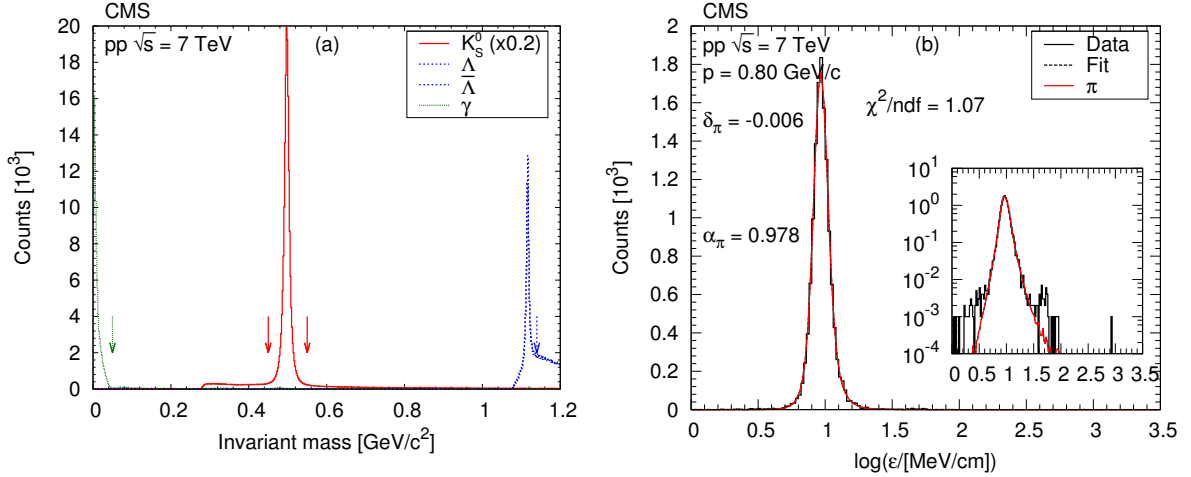


Figure 5: **(a)** Invariant mass distribution of K_S^0 , $\Lambda/\bar{\Lambda}$, and γ candidates. The K_S^0 histogram is multiplied by 0.2. Vertical arrows denote the chosen mass limits for candidate selection. **(b)** Example distribution of $\log \varepsilon$ in a narrow momentum slice at $p = 0.80 \text{ GeV}/c$ for the high-purity pion sample. Curves are template fits to the data, with scale factors (α) and shifts (δ) also given. The inset shows the distributions with a logarithmic vertical scale. Both plots are from data at 7 TeV center-of-mass energy.

tion, even for tracks with very few hits.

5 Fitting the $\log \varepsilon$ distributions

As seen in Fig. 4, low-momentum particles can be identified unambiguously and can therefore be counted. Conversely, at high momentum, the $\log \varepsilon$ bands overlap (above about $0.5 \text{ GeV}/c$ for pions and kaons, and $1.2 \text{ GeV}/c$ for protons); the particle yields therefore need to be determined by means of a series of template fits in bins of η and p_T . This is described in the following.

The starting point is the histogram of estimated $\log \varepsilon$ values m_i in a given (η, p_T) bin (i runs

over the histogram bins), along with normalised template distributions x_{ki} , with k indicating electron, pion, kaon, or proton. The goal is to determine the yield of each particle type (a_k) contributing to the measured distribution. Since the entries in a histogram are Poisson-distributed, the corresponding log-likelihood function to minimize is

$$\chi^2 = \sum_i 2 [t_i - m_i + m_i \log(m_i/t_i)], \quad (1)$$

where $t_i = \sum_k a_k x_{ki}$ contains the quantity to be fitted. The minimum for this non-linear expression can be found by using Newton's method [16], usually within three iterations. Although the templates describe the measured $\log \varepsilon$ distributions reasonably well, for a precision measurement further (track-level) corrections are needed to account for the remaining discrepancies between data and simulation. Hence, we allow for an affine transformation of the templates with scale factors and shifts that depend on η and p_T , the particle charge, and the particle mass.

For a less biased determination of track-level corrections, enhanced samples of each particle type were also employed. For electrons and positrons, photon conversions in the beam-pipe or in the first pixel layer were used. For high-purity π and enhanced p samples, weakly decaying hadrons were selected (K_S^0 , $\Lambda/\bar{\Lambda}$). Both photon conversions and weak decays were reconstructed by means of a simple neutral-decay finder, followed by a narrow mass cut. Invariant-mass distributions of the selected candidates are shown in Fig. 5a. A sample with enhanced kaon content was obtained by tagging K^\pm mesons (with the requirements listed in Table 3) and looking for an opposite-sign particle which, with the kaon mass assumption, would give an invariant mass close to that of the $\phi(1020)$, within $2\Gamma = 8.52 \text{ MeV}/c^2$. An example distribution of $\log \varepsilon$ for the high-purity pion sample in a narrow momentum slice is plotted in Fig. 5b.

5.1 Additional information for particle identification

At low momentum, the $\log \varepsilon$ templates for electrons and pions can be compared to the $\log \varepsilon$ distributions of high-purity samples, but this type of validation does not work at higher momenta because of lack of statistics; for the same reason, it does not work for kaons and protons. It is therefore important to study the $\log \varepsilon$ distributions in more detail: they contain useful additional information that can be used to determine the track-level corrections, thus reducing the systematic uncertainties of the extracted yields. This is discussed in the following.

a) Fitting $\log \varepsilon$ in n_{hits} slices. The n_{hits} distribution in a given (η, p_T) bin is different for different particle types. Pions have a higher average number of hits per track, with fewer hits for kaons and even fewer for protons. These differences are due to physical effects, such as the different inelastic hadron-nucleon cross section, multiple Coulomb scattering, and decay in flight. It is therefore advantageous to simultaneously perform differential fits in n_{hits} bins (Fig. 6a).

b) Fitting $\log \varepsilon$ in track-fit χ^2/ndf slices. The value of the global χ^2 per number of degrees of freedom (ndf) of the Kalman filter used for fitting the track [17], assuming the charged pion mass, can also be used to identify charged particles. Here ndf denotes the number of degrees of freedom for the track fit. This approach relies on the knowledge of the detector material and the local spatial resolution, and exploits the known physics of multiple scattering and energy loss; it can be used to enhance or suppress a specific particle type. The quantity $x = \sqrt{\chi^2/\text{ndf}}$ has an approximately Gaussian distribution with mean value 1 and standard deviation $\sigma \approx 1/\sqrt{2 \cdot \text{ndf}}$ if the track fitted is indeed a pion. If it is not, both the mean and sigma are larger by a factor $\beta(m_0)/\beta(m)$, where m_0 is the pion mass and m is the particle mass. Three classes were defined such that each contains an equal number of genuine pions. The condition $x -$

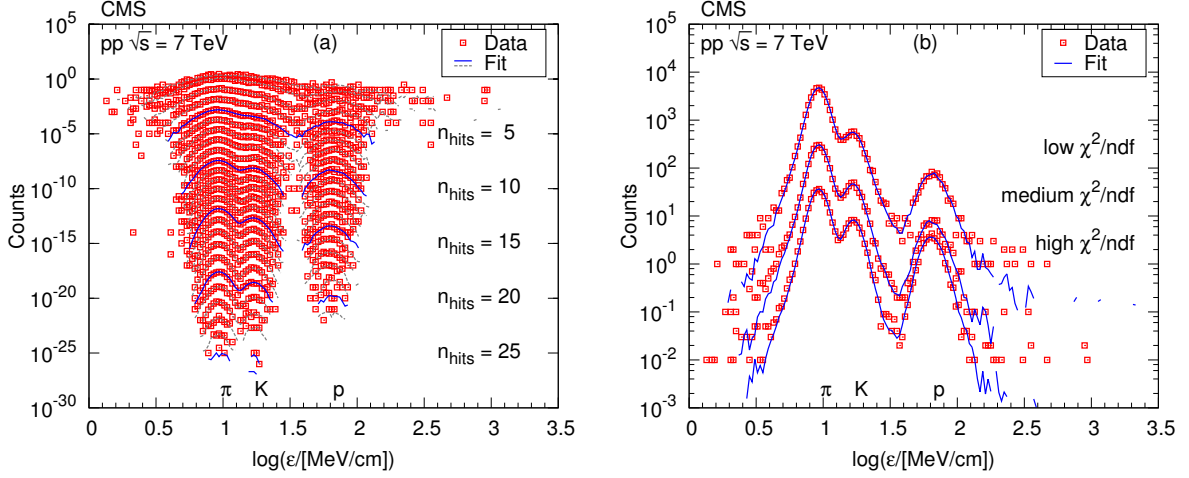


Figure 6: Examples of $\log \varepsilon$ distributions (symbols) for the 7 TeV dataset at $\eta = 0.35$, $p_T = 0.675 \text{ GeV}/c$, and corresponding template fits (solid curves represent the fit for the n_{hits} values indicated on the right, lighter dashed curves are for intermediate n_{hits}). The most probable values for pions (π), kaons (K), and protons (p) are indicated. **(a)** Distributions in n_{hits} slices. The points and the curves were scaled down by factors of $10^{-n_{\text{hits}}}$ for better visibility, with $n_{\text{hits}} = 1$ at the top. **(b)** Distributions in track-fit χ^2/ndf slices, integrated over all n_{hits} . The points and the curves were scaled down by factors of 1, 10, and 100 for better visibility, with the lowest χ^2/ndf slice at the top.

$1 < -0.43\sigma$ favors pions, and the requirements $-0.43\sigma \leq x - 1 < 0.43\sigma$ and $x - 1 \geq 0.43\sigma$ enhance kaons and protons, respectively. An example of $\log \varepsilon$ distributions in a χ^2/ndf slice, with the corresponding fits, is shown in Fig. 6b. The increase of the kaon and proton yields with increasing x is visible, when compared to pions.

c) Difference of hit losses. The n_{hits} distribution depends on the particle species, with pions producing more hits than other particles. Furthermore, the n_{hits} distributions of two particle types are related to each other. Let f_n denote the number of particles of type f with n hits ($n \geq 1$), in an (η, p_T) bin. Let us assume that another particle species g produces fewer hits, i.e. has a higher probability of hit loss q , taken to be roughly independent of the hit position along the track. The distribution of the number of hits g_k can then be predicted, with $g_k = r(1 - q)^k [f_k + q \sum_{n=k+1}^{\infty} f_n]$, where r is the ratio of particle abundances (g/f). The hit loss (compared to pions) is primarily a function of momentum. At lower momenta, the best value of q can be estimated for each (η, p_T) bin by comparing the measured kaon or proton distributions to the ones predicted with the pion n_{hits} distribution according to the formula above. An example of the n_{hits} distributions and the corresponding fits is shown in Fig. 7a. The resulting values of q as a function of p are shown in Fig. 7b, for the kaon-pion and proton-pion pairs. The data points with $q < 0.2$ can be approximated with a sum of two exponentials in p . This can be motivated by the decay in flight for kaons, but also by the increase of multiple Coulomb scattering with decreasing momentum. The weaker dependence at low momentum ($q > 0.2$) is due to the increasing multiple scattering for pions; however, this region is not used in the present analysis. The relation between the n_{hits} distributions of two particle types has very important consequences: since the number of charged particles at each n_{hits} value is known, only the local ratio r of particle abundances (K/π , p/π) has to be determined from the fits.

d) Continuity of parameters. In some (η, p_T) bins the track-level corrections (scale factors and shifts) are difficult to determine. These parameters are expected to change smoothly as the

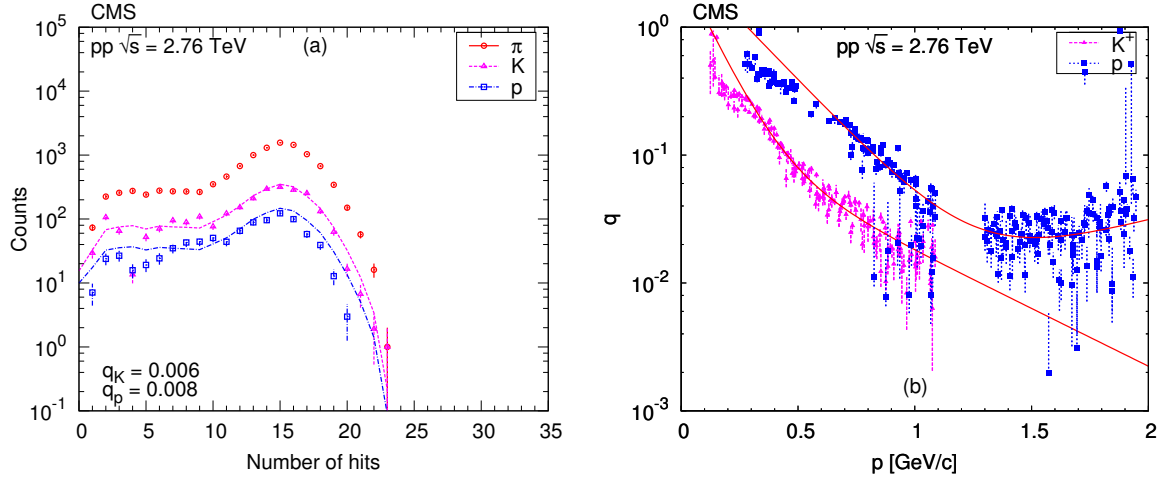


Figure 7: **(a)** Example of extracted n_{hits} distributions (symbols) of pions, kaons, and protons, for the 2.76 TeV dataset at $\eta = 0.35$, $p_T = 0.875 \text{ GeV}/c$, and corresponding fits (curves, see Section 5.1, paragraph c). **(b)** Probability of additional hit loss q with respect to pions as a function of total momentum p in the range $|\eta| < 1$ for positive kaons and protons, for the 2.76 TeV dataset, if the track-fit χ^2/ndf value is in the lowest slice. In order to exclude regions of crossing $\log \varepsilon$ bands, values are not shown if $p > 1.1 \text{ GeV}/c$ for kaons, and $1.1 < p < 1.3 \text{ GeV}/c$ for protons. These points were also omitted in the double-exponential fit.

kinematical region varies. The fit parameters are therefore smoothed by taking the median of the (η, p_T) bin and its 8 neighbors.

e) Convergence of parameters. While the track-level corrections are independent, they should converge to similar values at a momentum, p_c , where the ε values are the same for two particle types, although the energy deposit distributions can be slightly different. These momenta are $p_c = 1.56 \text{ GeV}/c$ for the pion-kaon and $2.58 \text{ GeV}/c$ for the pion-proton pair. The differences of fitted scale factors and shifts were studied as a function of $\Delta \log \varepsilon$, in narrow η slices. The parameter values were determined in the ranges $0.50 < p < 1.00 \text{ GeV}/c$ for kaons and $1.30 < p < 1.65 \text{ GeV}/c$ for protons. In these regions, the parameters were fitted and extrapolated to p_c . At p_c , the scale factors are expected to be the same and their $\Delta \log \varepsilon$ dependence is well described with first-order (proton-pion) or second-order polynomials (kaon-pion), in each η slice separately. More freedom had to be allowed for the shifts. While their $\Delta \log \varepsilon$ dependence can be described with first-order polynomials, their difference is not required to converge to 0, but to a second-order polynomial of η .

5.2 Determination of yields

In summary, in a given (η, p_T) bin, the free parameters are: the scale factors (usually in the range 0.98–1.02) and the shifts (from -0.01 to 0.01) for track-level corrections; the yields of particles for each χ^2/ndf bin or their ratios if the relationship between the n_{hits} distributions of different particle species is used. The fit was performed simultaneously in all $(n_{\text{hits}}, \chi^2/\text{ndf})$ bins with nested minimizations. The optimization of the parameters was carried out with the SIMPLEX package [18], but the determination of local particle yields was performed with the log-likelihood merit function (Eq. (1)).

In order to obtain a stable result, the fits were carried out in several passes, each containing iterative steps. After each step, the resulting scale factors and shifts were the new starting points for the next iteration. In the first pass, $\log \varepsilon$ distributions in narrow momentum slices were

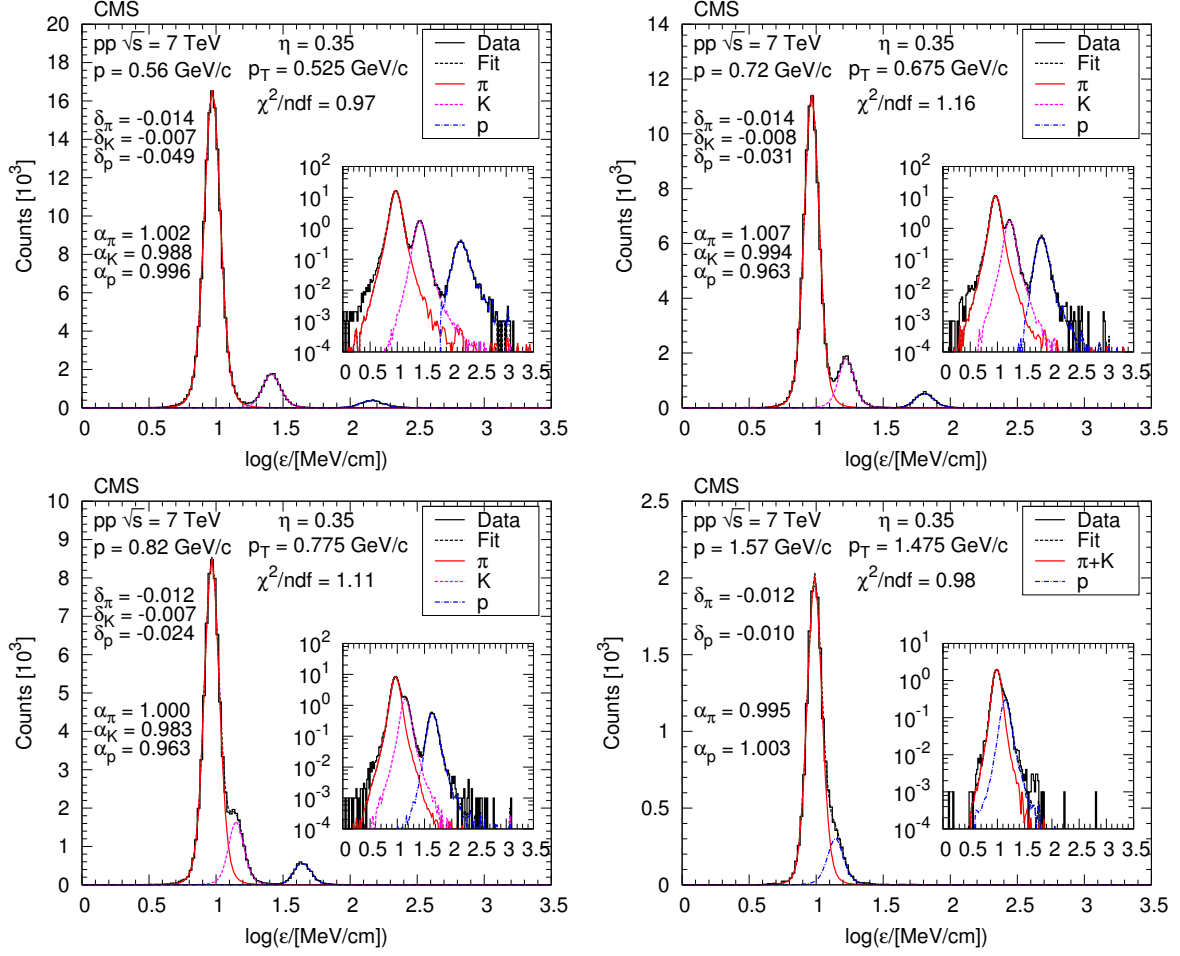


Figure 8: Example $\log \epsilon$ distributions at $\eta = 0.35$ in some selected p_T bins, for the 7 TeV dataset. The details of the template fits are discussed in the text. Scale factors (α) and shifts (δ) are indicated. The insets show the distributions with logarithmic vertical scale.

fitted using the enhanced electron, pion, proton, and kaon samples, as defined in Section 5. The fitted parameters were then used for a fit in the same slices of the inclusive dataset. In this way the scale factors and shifts were estimated as a function of p . In the second pass, the $\log \epsilon$ distributions in each (η, p_T) bin were fitted. The η bins are 0.1 units wide and cover the range $-2.4 < \eta < 2.4$. The p_T bins are 0.05 GeV/c wide and cover the range $p_T < 2$ GeV/c. The latter choice reflects the p_T resolution (0.015–0.025 GeV/c). The procedure was repeated with the enhanced samples, followed again by the inclusive sample. The n_{hits} distributions were used to extract the relationship between different particle species and this is used in all subsequent steps. The shifts are determined and constrained first, and then the scale factors are obtained. Example fits are shown in Fig. 8. In the last pass all parameters are kept constant and the final normalised $\log \epsilon$ templates for each particle species are extracted and used to measure the particle yields.

The results of the fitting sequence are the yields for each particle species and charge, both inclusive and divided into track multiplicity bins. While the yields are flat in η , they decrease with increasing p_T , as expected. At the end of the fitting sequence χ^2/ndf values are usually close to unity, except for some low- p_T fits. At low p the pions are well fitted, and the different species are well separated. Hence, instead of fitting kaon or proton yields, it is sufficient to

Table 4: Momentum ranges used in various steps and procedures of the analysis. Total momentum values are given in GeV/c. The use of hit loss and parameter convergence is with respect to π for K, and π +K for p.

<i>Particle</i>	<i>Count</i>	<i>Fit</i>	<i>Hit loss</i>	<i>Convergence</i>	<i>Physics</i>
e		$p < 0.15$			$0.10 < p < 0.15$
π		$p < 1.30$		$0.95 < p < 1.30$	$0.10 < p < 1.20$
π +K		$1.30 < p < 1.95$			$1.05 < p < 1.50$
K	$0.12 < p < 0.27$	$0.20 < p < 1.30$	$p > 0.70$	$0.95 < p < 1.30$	$0.20 < p < 1.05$
p	$0.27 < p < 0.70$	$0.30 < p < 1.95$	$p > 1.45$	$1.60 < p < 1.95$	$0.35 < p < 1.70$

count the number of entries above the fitted shape of the pion distribution.

Table 4 summarizes the particle-specific momentum ranges for the following procedures: counting the yields (*Count*); using a particle species in the fits (*Fit*, paragraphs a and b in Section 5.1); using the correspondence between hit losses in the fits (*Hit loss*, paragraph c); using the principle of convergence for track-level corrections in the fits (*Convergence*, paragraph e); and using the fitted yields for physics (*Physics*). The use of these ranges limits the systematic uncertainties at high momentum. The ranges, after evaluation of the individual fits, were set such that the systematic uncertainty of the measured yields does not exceed 10%. For $p > 1.30$ GeV/c, pions and kaons were not fitted separately, but were regarded as one particle species (π +K row in Table 4). In fact, fitted pion and kaon yields were not used for $p > 1.20$ GeV/c and $p > 1.05$ GeV/c, respectively. Although pion and kaon yields cannot be determined in this high-momentum region, their sum can be measured. This information is an important constraint when fitting the p_T spectra (Section 7).

The statistical uncertainties for the extracted yields are given by the fits. The observed local (η, p_T) variations of parameters for track-level corrections cannot be attributed to statistical fluctuations and indicate that the average systematic uncertainties of the scale factors and shifts are about 10^{-2} and $2 \cdot 10^{-3}$, respectively. The systematic uncertainties on the yields in each bin were obtained by refitting the histograms with the parameters changed by these amounts.

6 Corrections

The measured yields in each (η, p_T) bin, $\Delta N_{\text{measured}}$, were first corrected for the misreconstructed-track rate (C_f , Section 3.2) and the fraction of secondaries (C_s , Section 3.3):

$$\Delta N' = \Delta N_{\text{measured}} \cdot (1 - C_f) \cdot (1 - C_s). \quad (2)$$

Bins in which the misreconstructed-track rate was larger than 0.1 or the fraction of secondaries was larger than 0.25 were rejected.

The distributions were then unfolded to take into account the finite η and p_T resolutions. The η distribution of the tracks is flat and the η resolution is very good. Conversely, the p_T distribution is steep in the low-momentum region and separate corrections in each η bin were necessary. In addition, the reconstructed p_T distributions for kaons and protons, at very low p_T , are shifted with respect to the generated distributions by about 0.025 GeV/c. This bias is a consequence of using the pion mass for all charged particles (see Section 5.1). A straightforward unfolding procedure with linear regularization [16] was used, based on response matri-

ces R obtained from MC samples for each particle species. With \mathbf{o} and \mathbf{m} denoting the vector of original and measured differential yields ($d^2N/d\eta dp_T$), the sum of the chi-squared term $(R\mathbf{o} - \mathbf{m})^T V^{-1} (R\mathbf{o} - \mathbf{m})$ and a regularizer term $\lambda \mathbf{o}^T H \mathbf{o}$ is minimized by varying \mathbf{o} , where H is a tridiagonal matrix. The covariance of measured values is approximated by $V_{ij} \approx m_i \delta_{ij}$, where δ_{ij} is Kronecker's delta. The value of λ is adjusted such that the minimized sum of the two terms equals the number of degrees of freedom. In practice the parameter λ is small, of the order of 10^{-5} .

The corrected yields were obtained by applying corrections (cf. Section 3.2) for acceptance (C_a), efficiency (C_e), and multiple reconstruction rate (C_m):

$$\frac{1}{N_{\text{ev}}} \frac{d^2N}{d\eta dp_T}_{\text{corrected}} = \frac{1}{C_a \cdot C_e \cdot (1 + C_m)} \frac{\Delta N'}{N_{\text{ev}} \Delta\eta \Delta p_T}, \quad (3)$$

where N_{ev} is the corrected number of DS events (see Section 3). Bins with acceptance smaller than 0.5, efficiency smaller than 0.5, or multiple-track rate greater than 0.1 were rejected.

Finally, the differential yields $d^2N/d\eta dp_T$ were transformed to invariant yields as a function of the rapidity y by multiplying by the Jacobian E/p , and the (η, p_T) bins were mapped into a (y, p_T) grid. The invariant yields $1/N_{\text{ev}} d^2N/dy dp_T$ as a function of p_T were obtained by averaging over y in the range $-1 < y < 1$. They are largely independent of y in the narrow region considered, as expected.

6.1 Systematic uncertainties

The systematic uncertainties are summarized in Table 5; they are subdivided in three categories.

- The uncertainties of the corrections related to the event selection (Section 3.1) and pileup (Section 3.3) are fully or mostly correlated and were treated as normalisation uncertainties. They amount to a 3.0% systematic uncertainty on the yields and 1.0% on the average p_T .
- The pixel hit efficiency and the effects of a possible misalignment of the detector elements are mostly uncorrelated. Their contribution to the yield uncertainty is about 0.3% [7].
- Other mostly uncorrelated systematic effects are the following: the tracker acceptance and the track reconstruction efficiency (Section 3.2) generally have small uncertainties (1% and 2%, respectively), but change rapidly at very low p_T , leading to a 5–6% uncertainty on the yields in that range; for the multiple-track and misreconstructed-track rate corrections (Section 3.2), the uncertainty is assumed to be 50% of the correction, while for the case of the correction for secondary particles it is 20% (Section 3.3). The uncertainty of the fitted yields (Section 5.2) also belongs to this category.

In the weighted averages and the fits discussed in the following, the quadratic sum of statistical and systematic uncertainties (referred to as combined uncertainty) is used. The fully correlated systematic uncertainties (event selection and pileup) are not displayed in the plots.

7 Results

In previously published measurements of unidentified and identified particle spectra, the following form of the Tsallis-Pareto-type distribution [19, 20] was fitted to the data:

Table 5: Summary of the systematic uncertainties on the spectra. Values in parentheses indicate uncertainties on the $\langle p_T \rangle$ measurement. Representative, particle-specific uncertainties (π , K, p) are shown at $p_T = 0.6$ GeV/c.

Source	Uncertainty of the source [%]	Propagated yield uncertainty [%]		
Fully correlated, normalisation				
Correction for event selection	3.0 (1.0)	}	3.0 (1.0)	
Pileup correction (merged and split vertices)	0.3			
Mostly uncorrelated				
Pixel hit efficiency	0.3	}	0.3	
Misalignment, different scenarios	0.1			
Mostly uncorrelated, (y, p_T) dependent		π	K	p
Acceptance of the tracker	1–6	1	1	1
Efficiency of the reconstruction	2–5	2	2	2
Multiple-track reconstruction	50% of the corr.	–	–	–
Misreconstructed-track rate	50% of the corr.	<0.5	<0.5	0.5
Correction for secondary particles	20% of the corr.	<0.5	–	2
Fitting log ε distributions	1–10	1	2	1

$$\frac{d^2N}{dydp_T} = \frac{dN}{dy} \cdot C \cdot p_T \left[1 + \frac{(m_T - m)}{nT} \right]^{-n}, \quad (4)$$

where

$$C = \frac{(n-1)(n-2)}{nT[nT + (n-2)m]} \quad (5)$$

and $m_T = \sqrt{m^2 + p_T^2}$ (c factors are omitted from the preceding formulae). The free parameters are the integrated yield dN/dy , the exponent n , and the inverse slope T . The above formula is useful for extrapolating the spectra to $p_T = 0$, and for extracting $\langle p_T \rangle$ and dN/dy . Its validity in the present analysis was cross-checked by fitting MC spectra and verifying that the fitted values of $\langle p_T \rangle$ and dN/dy were consistent with the generated values. According to some models of particle production based on non-extensive thermodynamics [20], the parameter T is connected with the average particle energy, while n characterizes the “non-extensivity” of the process, i.e. the departure of the spectra from a Boltzmann distribution.

As discussed earlier, pions and kaons cannot be unambiguously distinguished at higher momenta (Section 5.2). Because of this, the pion-only (kaon-only) $d^2N/dydp_T$ distribution was fitted for $|y| < 1$ and $p < 1.20$ GeV/c ($p < 1.05$ GeV/c); the joint pion and kaon distribution was instead fitted if $|\eta| < 1$ and $1.05 < p < 1.5$ GeV/c. Since the ratio p/E for the pions (which are more abundant than kaons) at these momenta can be approximated by p_T/m_T at $\eta \approx 0$, Eq. (4) becomes:

$$\frac{d^2N}{d\eta dp_T} \approx \frac{dN}{dy} \cdot C \cdot \frac{p_T^2}{m_T} \left(1 + \frac{m_T - m}{nT} \right)^{-n}. \quad (6)$$

In the case of pions and protons, the measurements cover a wide p_T range: the yields and average p_T can thus be determined with small systematic uncertainty. For the kaons the number of measurements is small and the p_T range is limited. Therefore, for the combined pion and kaon fits, the kaon component was weighted by a factor of four, leading to the following function to be minimized: $\chi_\pi^2 + \chi_{\pi+K}^2 + 4\chi_K^2$. This weight accounts for the p_T range, which is narrower by a factor about two, and also for the partial correlation between the pion measurement and that of the sum of pions and kaons, which gives another factor two.

The average transverse momentum $\langle p_T \rangle$ and its uncertainty were obtained by numerical integration of Eq. (4) with the fitted parameters.

The results discussed in the following are for $|y| < 1$ at $\sqrt{s} = 0.9, 2.76$, and 7 TeV. In all cases, error bars indicate the uncorrelated statistical uncertainties, while bands show the uncorrelated systematic uncertainties. The fully correlated normalisation uncertainty (not shown) is 3.0%. For the p_T spectra, the average transverse momentum, and the ratio of particle yields, the data are compared to the D6T and Z2 tunes of PYTHIA6 [8] as well as to the 4C tune of PYTHIA8 [21].

7.1 Inclusive measurements

The transverse momentum distributions of positive and negative hadrons (pions, kaons, protons) are shown in Fig. 9, along with the results of the fits to the Tsallis-Pareto parametrization (Eqs. (4) and (6)). The fits are of good quality with χ^2/ndf values in the range 0.6–1.5 for pions, 0.6–2.1 for kaons, and 0.4–1.1 for protons. Figure 10 presents the data compared to various PYTHIA tunes. Tunes D6T and 4C tend to be systematically below or above the spectra, whereas Z2 is generally closer to the measurements (except for low- p_T protons).

Ratios of particle yields as a function of the transverse momentum are plotted in Fig. 11. While the p/π ratios are well described by all tunes, there are substantial deviations for the K/π ratios, also seen by other experiments and at different energies. CMS measurements of K_S^0 and $\Lambda/\bar{\Lambda}$ production [14] are consistent with the discrepancies seen here. The ratios of the yields for oppositely charged particles are close to one, as expected for pair-produced particles at midrapidity. Ratios for pions and kaons are compatible with unity, independently of p_T . While the \bar{p}/p ratios are also flat as a function of p_T , they increase with increasing \sqrt{s} .

7.2 Multiplicity-dependent measurements

This study is motivated by the intriguing hadron correlations measured in pp collisions at high track multiplicities [22], which suggest possible collective effects in “central” pp collisions at the LHC. In addition, the multiplicity dependence of particle yield ratios is sensitive to various final-state effects (hadronization, color reconnection, collective flow) implemented in MC models used in collider and cosmic-ray physics [23].

Twelve event classes were defined, each with a different number of reconstructed particles: $N_{\text{rec}} = (0-9), (10-19), (20-29), \dots, (100-109)$ and $(110-119)$, as shown in Table 6. In order to facilitate comparisons with models, the corresponding true track multiplicity in the range $|\eta| < 2.4$ (N_{tracks}) was determined from the simulation. The average $\langle N_{\text{tracks}} \rangle$ values, given in Table 6, are used in the plots presented in the following. The results in the table were found to be independent of the center-of-mass energy and the PYTHIA tune.

The normalized transverse-momentum distributions of identified charged hadrons in selected multiplicity classes, for $|y| < 1$ and $\sqrt{s} = 0.9, 2.76$, and 7 TeV, are shown in Figs. 12, 13, and 14, for pions, kaons, and protons, respectively. The distributions of negatively and positively charged particles have been summed. The distributions are fitted to the Tsallis-Pareto

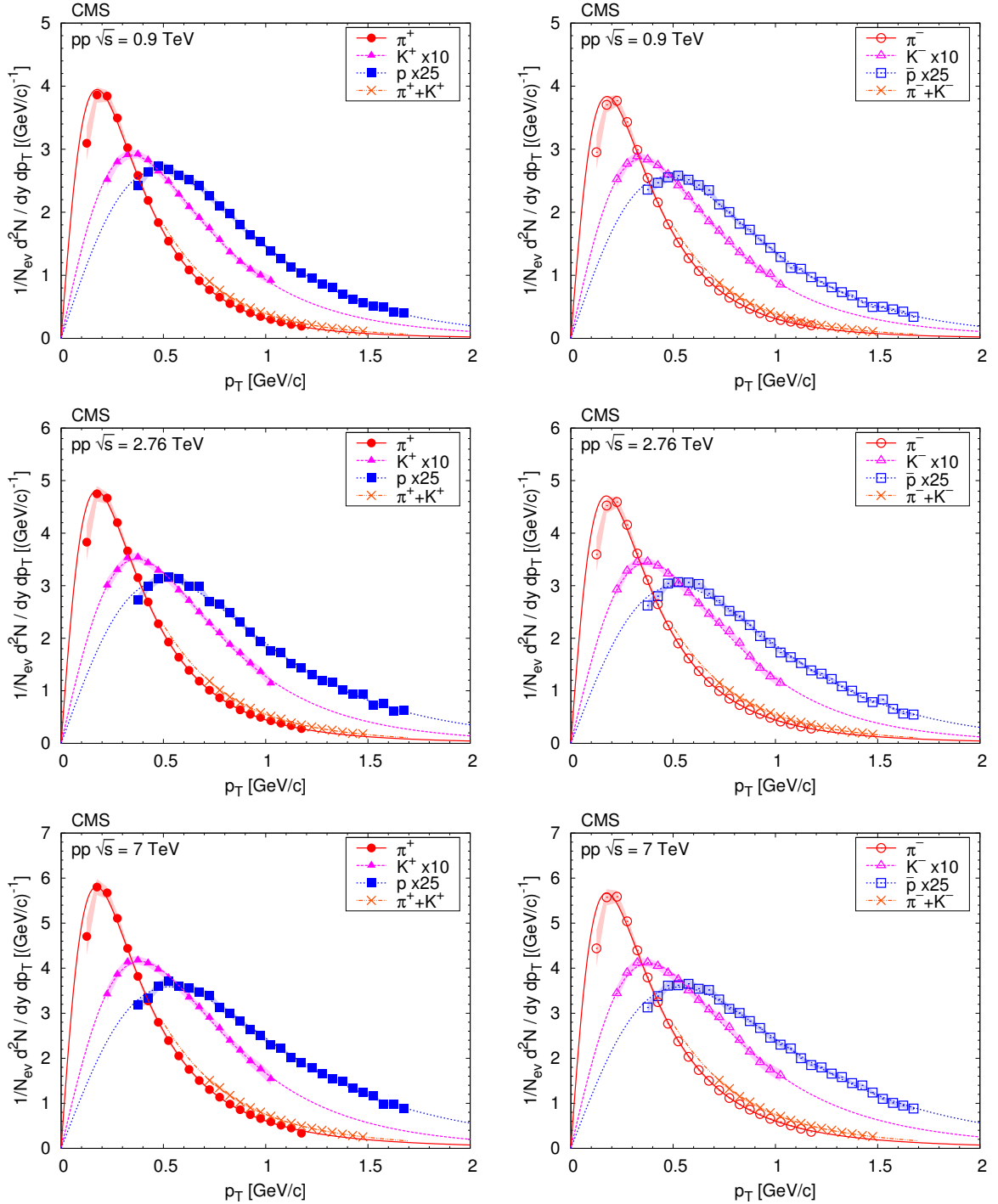


Figure 9: Transverse momentum distributions of identified charged hadrons (pions, kaons, protons) in the range $|y| < 1$, for positive (left) and negative (right) particles, at $\sqrt{s} = 0.9$, 2.76, and 7 TeV (from top to bottom). Kaon and proton distributions are scaled as shown in the legends. Fits to Eq. (4) are superimposed. Error bars indicate the uncorrelated statistical uncertainties, while bands show the uncorrelated systematic uncertainties. The fully correlated normalisation uncertainty (not shown) is 3.0%.

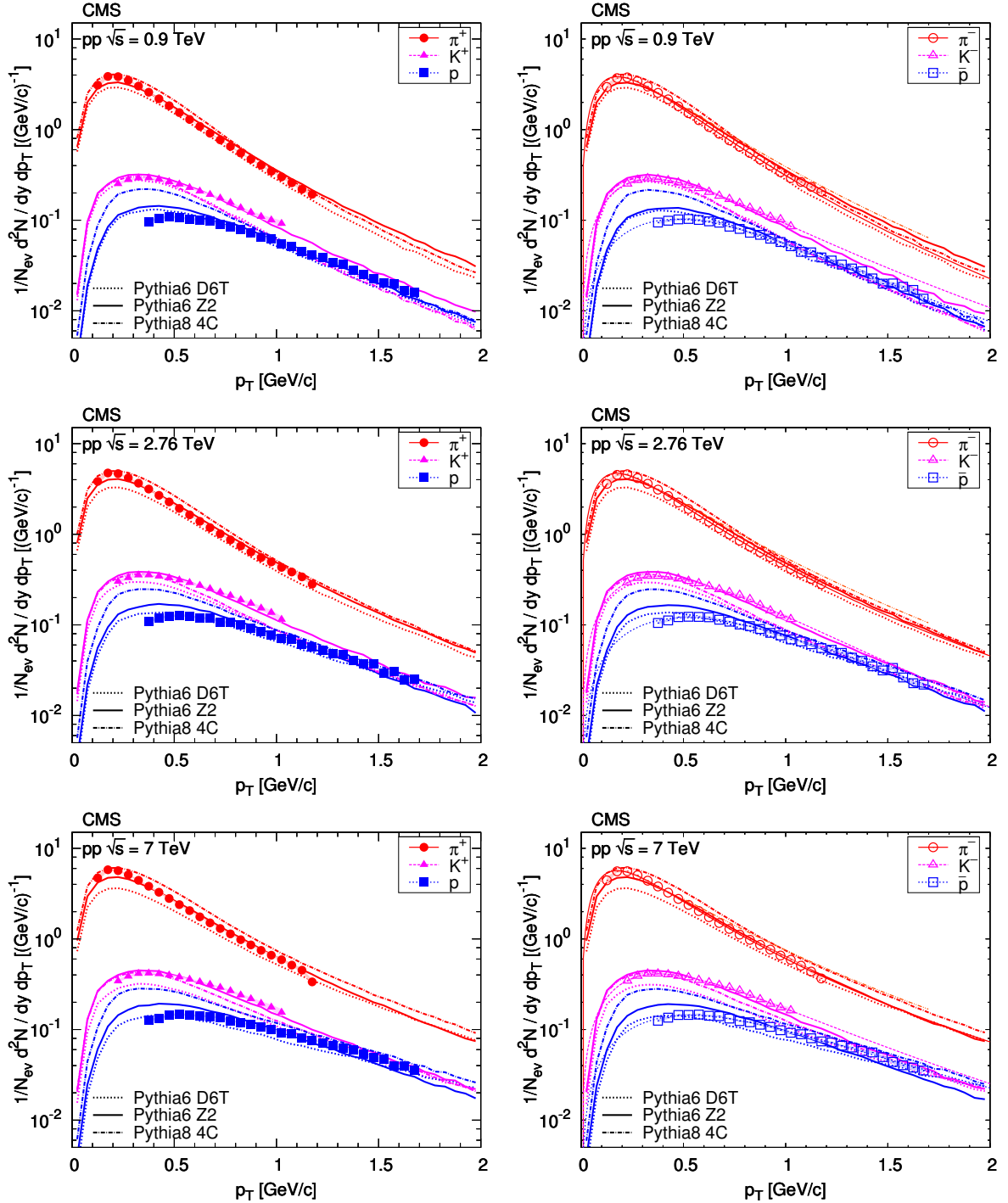


Figure 10: Transverse momentum distributions of identified charged hadrons (pions, kaons, protons) in the range $|y| < 1$, for positive (left) and negative (right) particles, at $\sqrt{s} = 0.9, 2.76$, and 7 TeV (from top to bottom). Measured values (same as in Fig. 9) are plotted together with predictions from PYTHIA6 (D6T and Z2 tunes) and the 4C tune of PYTHIA8. Error bars indicate the uncorrelated statistical uncertainties, while bands show the uncorrelated systematic uncertainties. The fully correlated normalisation uncertainty (not shown) is 3.0%.

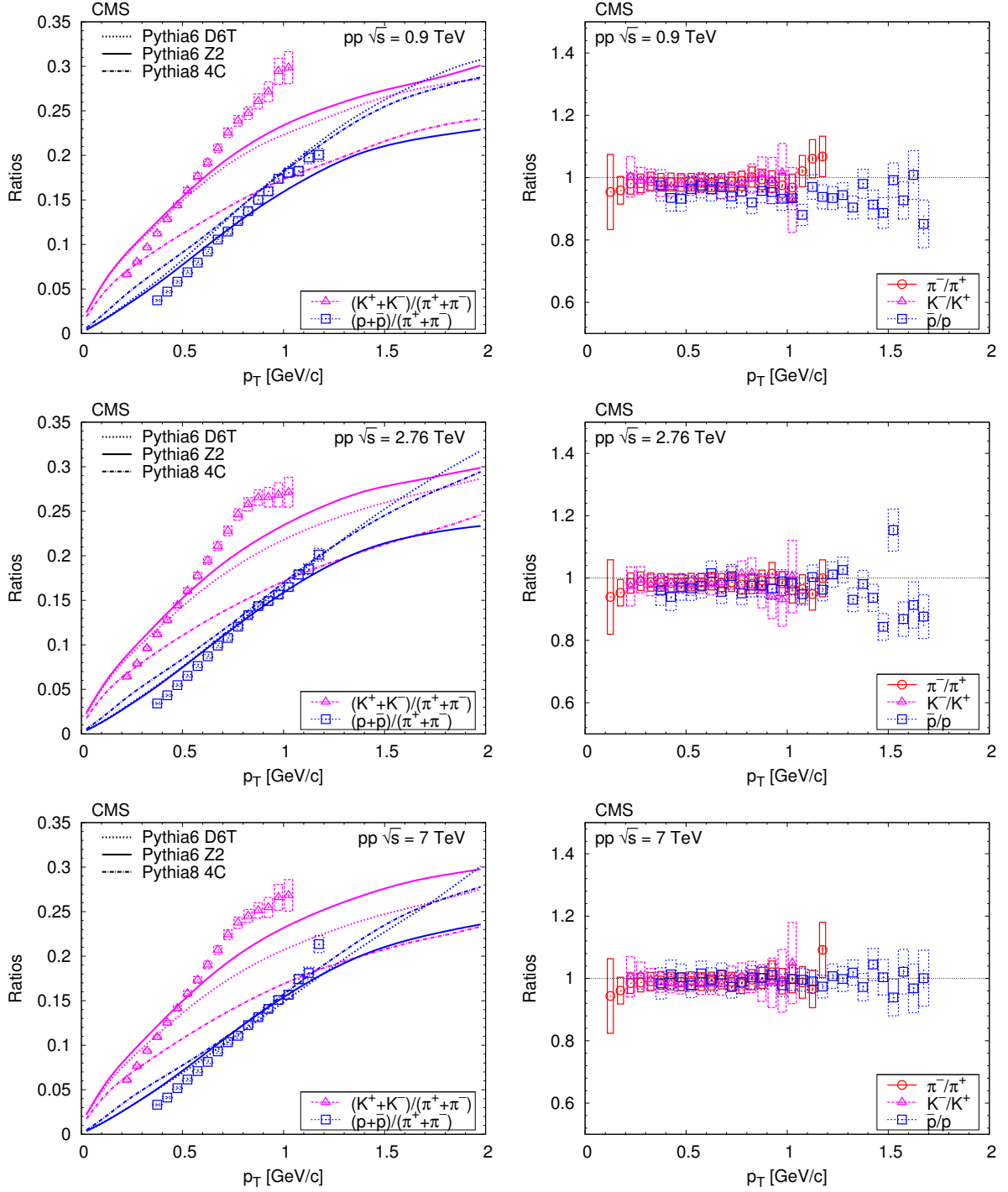


Figure 11: Ratios of particle yields as a function of transverse momentum, at $\sqrt{s} = 0.9, 2.76$, and 7 TeV (from top to bottom). Error bars indicate the uncorrelated statistical uncertainties, while boxes show the uncorrelated systematic uncertainties. Curves indicate predictions from PYTHIA6 (D6T and Z2 tunes) and the 4C tune of PYTHIA8.

Table 6: Relationship between the number of reconstructed tracks (N_{rec}) and the average number of true tracks ($\langle N_{\text{tracks}} \rangle$) in the 12 multiplicity classes considered.

N_{rec}	0-9	10-19	20-29	30-39	40-49	50-59	60-69	70-79	80-89	90-99	100-109	110-119
$\langle N_{\text{tracks}} \rangle$	7	16	28	40	52	63	75	86	98	109	120	131

parametrization. In the case of pions, the distributions are remarkably similar, and essentially independent of \sqrt{s} and multiplicity. For kaons and protons, there is a clear evolution as the multiplicity increases. The inverse slope parameter T increases with multiplicity for both kaons and protons, while the exponent n is independent of the multiplicity (not shown in the figures).

The ratios of particle yields as a function of track multiplicity are displayed in Fig. 15. The K/π and p/π ratios are flat as a function of N_{tracks} . Although the trend at low N_{tracks} is not reproduced by any of the tunes, the values are approximately correct for tunes D6T and Z2, while 4C is off, especially for K/π . The ratios of yields of oppositely charged particles are independent of N_{tracks} .

The average transverse momentum $\langle p_T \rangle$ is shown as a function of multiplicity in Fig. 16. The plots are similar, and largely independent of \sqrt{s} , for all the particle species studied. Pions and kaons are well described by the Z2 and 4C tunes, while D6T predicts values that are too high at high multiplicities. None of the tunes provide an acceptable description of the multiplicity dependence of $\langle p_T \rangle$ for protons, and the measured values lie between D6T and Z2. For the dependence of T on multiplicity (not shown in the figures), the predictions are consistently higher than the pion data for all tunes; the kaon and proton data are again between D6T and Z2, somewhat closer to the latter. Tune 4C gives a flat multiplicity dependence for T and is not favored by the kaon and proton measurements.

The center-of-mass energy dependence of dN/dy , the average transverse momentum $\langle p_T \rangle$, and the particle yield ratios are shown in Fig. 17. For dN/dy , the Z2 tune gives the best overall description. The $\langle p_T \rangle$ of pions is reproduced by tune 4C, that of the kaons is best described by Z2, and that of the protons is not reproduced by any of the tunes, with D6T closest to the data. The ratios of the yields for oppositely charged mesons are independent of \sqrt{s} and have values of about 0.98 for the pions; the kaon ratios are compatible with those of the pion and also with unity. The slight deviation from unity observed for the pions probably reflects the initial charge asymmetry of pp collisions. The \bar{p}/p yield ratio appears to increase with \sqrt{s} , though it is difficult to draw definite conclusions because of the large systematic uncertainties. The K/π and p/π ratios are flat as a function of \sqrt{s} , and have values of 0.13 and 0.06–0.07, respectively. The exponent n (not shown in the figures) decreases with increasing \sqrt{s} for pions and protons. For the kaons the systematic uncertainties are too large to draw a definite conclusion. The inverse slope T (also not shown) is flat as a function of \sqrt{s} for the pions but exhibits a slight increase for the protons. The universality of the relation of $\langle p_T \rangle$ and the particle-yield ratios with the track multiplicity, and its independence of the collision energy is demonstrated in Fig. 18.

The transverse-momentum distributions of identified charged hadrons at central rapidity are compared to those of the ALICE Collaboration [24] at $\sqrt{s} = 0.9$ TeV in Fig. 19 ($|y| < 1$ for CMS, $|y| < 0.5$ for ALICE). While the rapidity coverage is different, the measurements can be compared because the p_T spectra are largely independent of y for $|y| < 1$. The results from

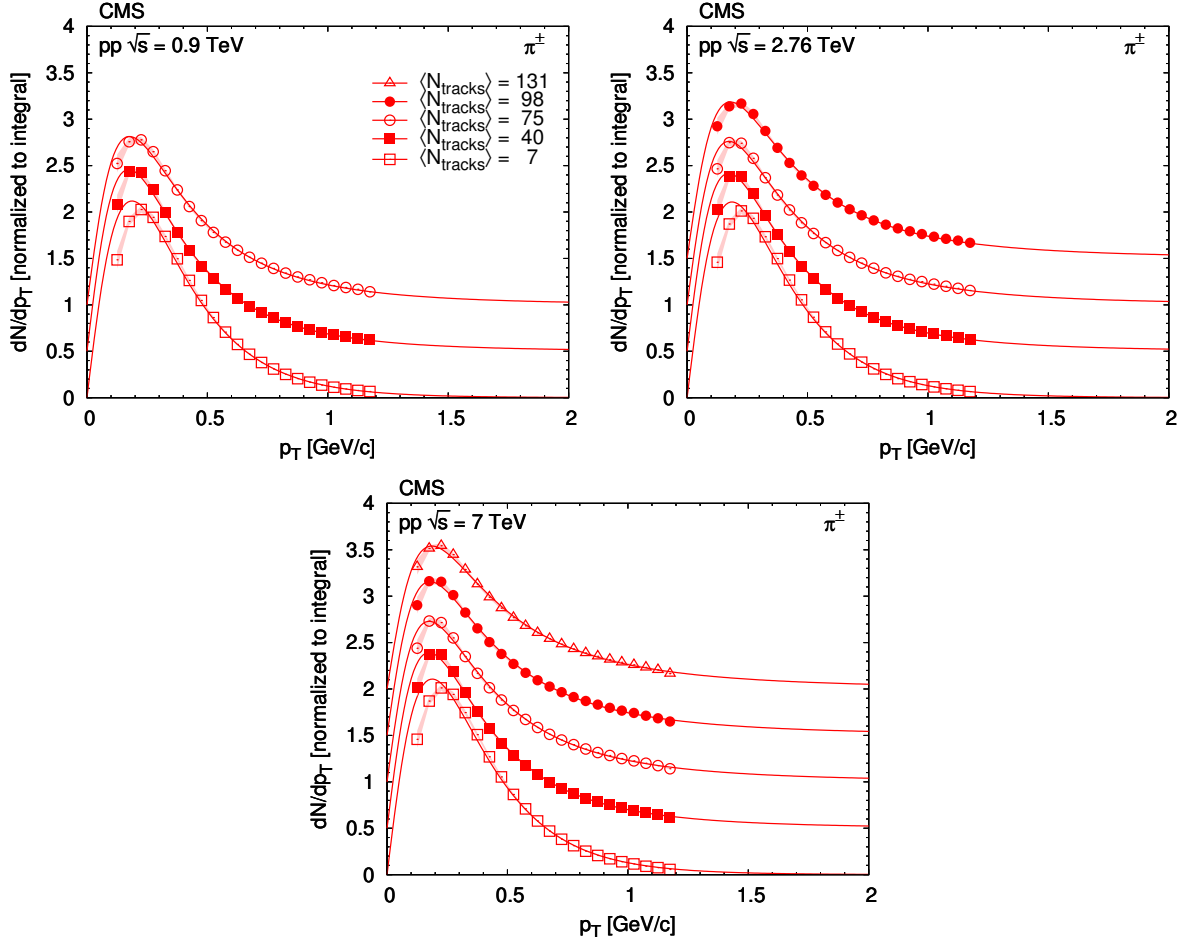


Figure 12: Normalized transverse momentum distributions of charged pions in a few representative multiplicity classes, in the range $|y| < 1$, at $\sqrt{s} = 0.9, 2.76$, and 7 TeV, fitted to the Tsallis-Pareto parametrization (solid lines). For better visibility, the result for any given $\langle N_{\text{tracks}} \rangle$ bin is shifted by 0.5 units with respect to the adjacent bins. Error bars indicate the uncorrelated statistical uncertainties, while bands show the uncorrelated systematic uncertainties.

the two experiments agree well for the mesons, and exhibit some small discrepancies for the protons.

The center-of-mass energy dependence of dN/dy in the central rapidity region and the average transverse momentum for pions, kaons, and protons are shown in Fig. 20. Measurements from UA2 [25], E735 [26], PHENIX [27], STAR [28], ALICE [24], and CMS are shown. The observed \sqrt{s} evolution of both quantities is consistent with a power-law increase.

The comparison of the central rapidity \bar{p}/p ratio as a function of the rapidity interval Δy is displayed in Fig. 21. This quantity is defined as $\Delta y = y_{\text{beam}} - y_{\text{baryon}}$, where y_{beam} (y_{baryon}) is the rapidity of the incoming beam (outgoing baryon). Measurements from ISR energies [29, 30], NA49 [31], BRAHMS [32], PHENIX [33], PHOBOS [34], and STAR [35] are shown together with LHC (ALICE [36] and CMS) data. The curve represents the expected Δy dependence in a Regge-inspired model, where baryon pair production is governed by Pomeron exchange, and baryon transport by string-junction exchange [37]. The functional form used is $(\bar{p}/p)^{-1} = 1 + C \exp[(\alpha_J - \alpha_P)\Delta y]$ with $C = 10$, $\alpha_P = 1.2$, and $\alpha_J = 0.5$, as used in the ALICE paper. While the low Δy region is not properly described, the agreement is good at higher Δy . The CMS data

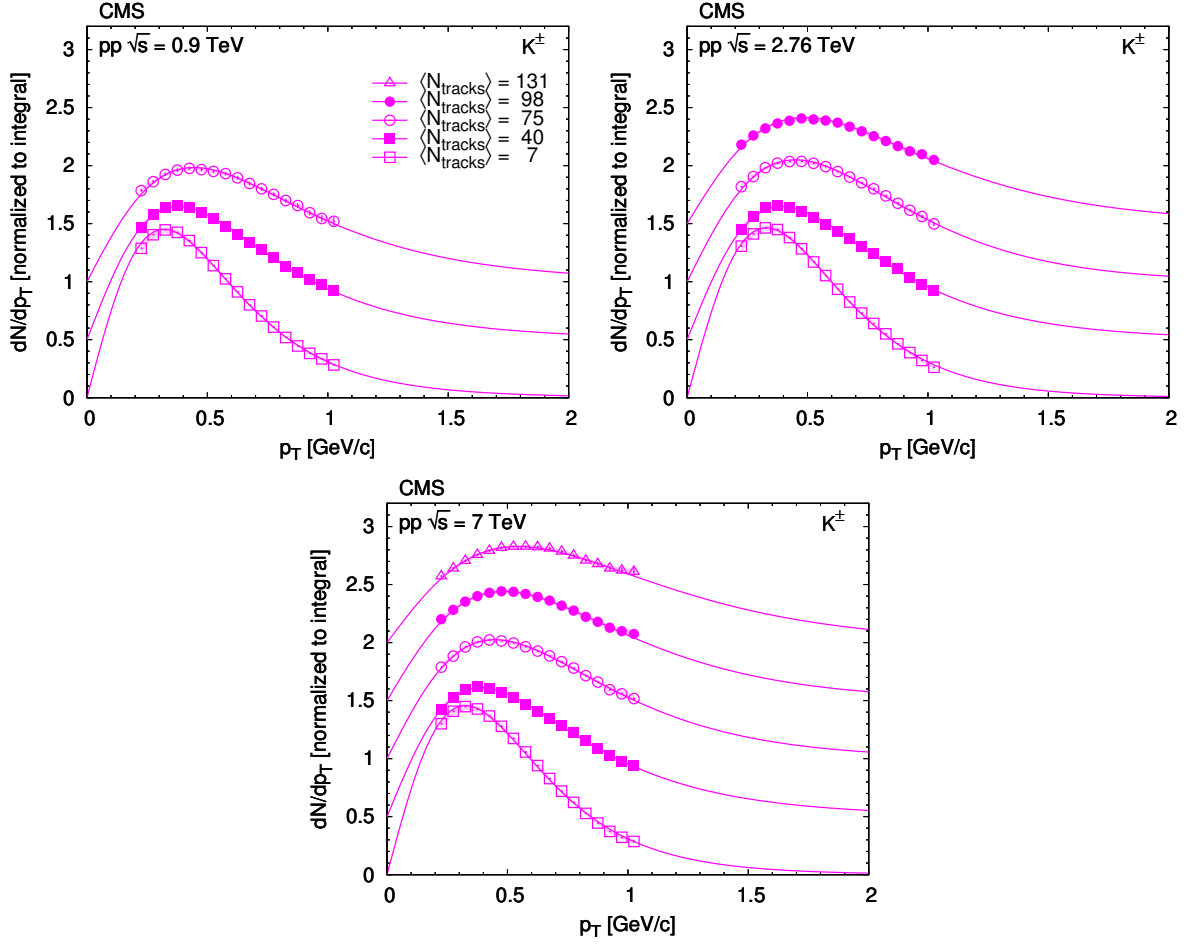


Figure 13: Normalized transverse momentum distributions of charged kaons in a few representative multiplicity classes, in the range $|y| < 1$, at $\sqrt{s} = 0.9, 2.76$, and 7 TeV, fitted to the Tsallis-Pareto parametrization (solid lines). For better visibility, the result for any given $\langle N_{\text{tracks}} \rangle$ bin is shifted by 0.5 units with respect to the adjacent bins. Error bars indicate the uncorrelated statistical uncertainties, while bands show the uncorrelated systematic uncertainties.

are consistent with previous measurements, as well as with the proposed function. New data from the LHCb Collaboration [38] in the forward region could further constrain the parameters of the model.

8 Conclusions

Measurements of identified charged hadrons produced in pp collisions at $\sqrt{s} = 0.9, 2.76$, and 7 TeV have been presented, based on data collected in events with simultaneous hadronic activity at pseudorapidities $-5 < \eta < -3$ and $3 < \eta < 5$. Charged pions, kaons, and protons were identified from the energy deposited in the silicon tracker (pixels and strips) and other track information (number of hits and goodness of track-fit). CMS data extend the center-of-mass energy range of previous measurements and are consistent with them at lower energies. Moreover, in the present analysis the data have been studied differentially, as a function of the particle multiplicity in the event and of the collision energy. The results can be used to further constrain models of hadron production and contribute to the understanding of basic non-perturbative dynamics in hadronic collisions.

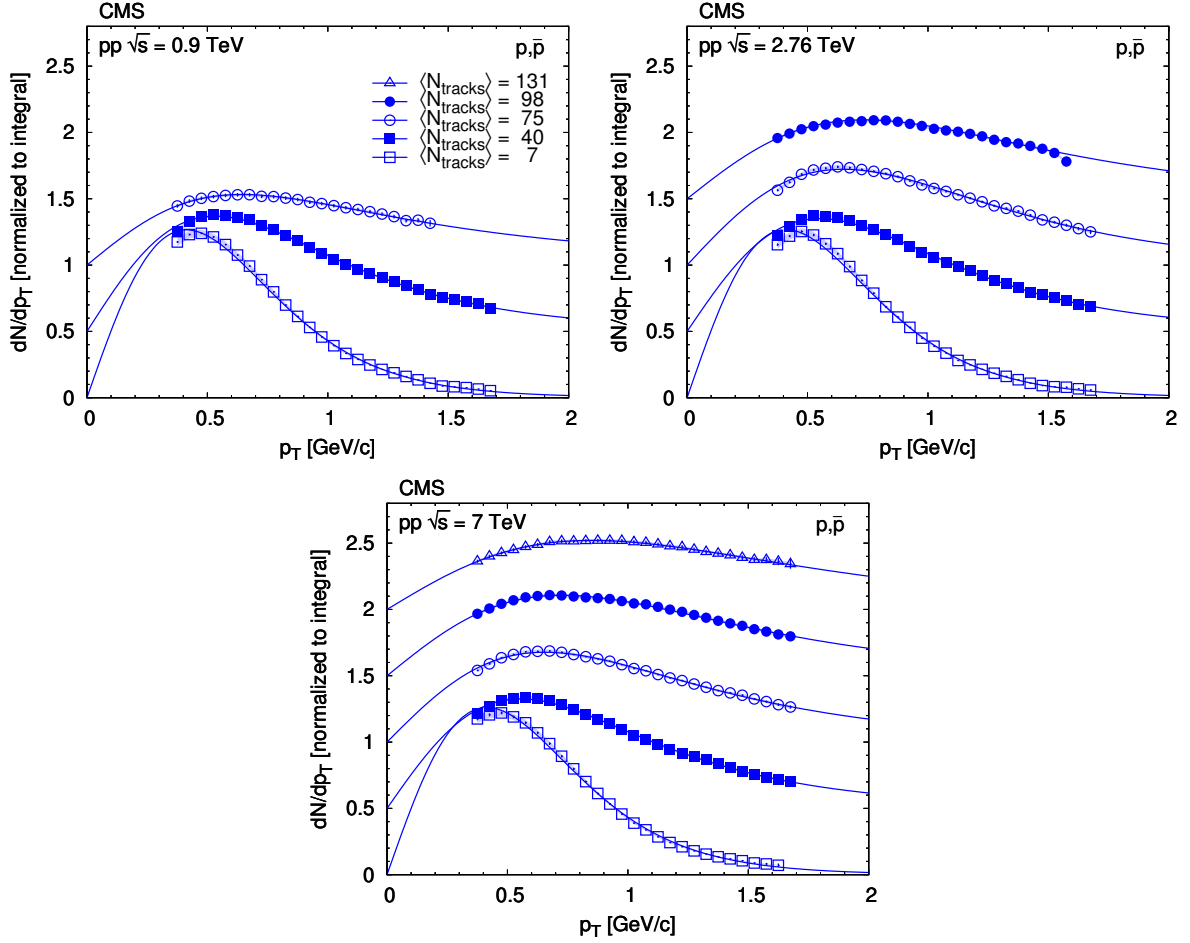


Figure 14: Normalized transverse momentum distributions of charged protons in a few representative multiplicity classes, in the range $|y| < 1$, at $\sqrt{s} = 0.9, 2.76$, and 7 TeV, fitted to the Tsallis-Pareto parametrization (solid lines). For better visibility, the result for any given $\langle N_{\text{tracks}} \rangle$ bin is shifted by 0.5 units with respect to the adjacent bins. Error bars indicate the uncorrelated statistical uncertainties, while bands show the uncorrelated systematic uncertainties.

The measured track multiplicity dependence of the rapidity density and of the average transverse momentum indicates that particle production at LHC energies is strongly correlated with event particle multiplicity rather than with the center-of-mass energy of the collision. This correlation may reflect the fact that at TeV energies the characteristics of particle production in hadronic collisions are constrained by the amount of initial parton energy available in a given collision.

Acknowledgments

We congratulate our colleagues in the CERN accelerator departments for the excellent performance of the LHC machine. We thank the technical and administrative staff at CERN and other CMS institutes. This work was supported by the Austrian Federal Ministry of Science and Research; the Belgium Fonds de la Recherche Scientifique, and Fonds voor Wetenschappelijk Onderzoek; the Brazilian Funding Agencies (CNPq, CAPES, FAPERJ, and FAPESP); the Bulgarian Ministry of Education and Science; CERN; the Chinese Academy of Sciences, Ministry of Science and Technology, and National Natural Science Foundation of China; the Colom-

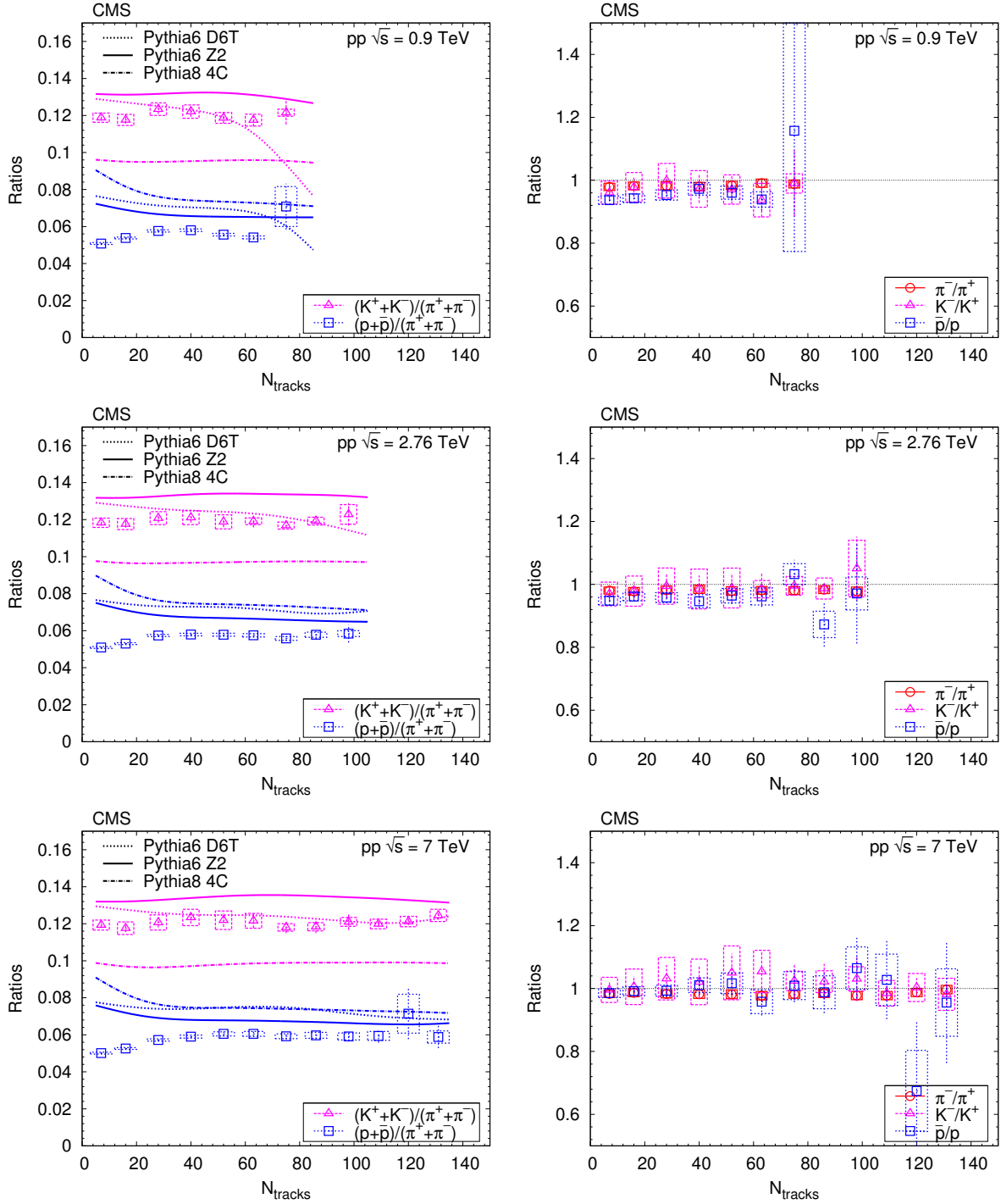


Figure 15: Ratios of particles yields in the range $|y| < 1$ as a function of the true track multiplicity for $|\eta| < 2.4$, at $\sqrt{s} = 0.9, 2.76$, and 7 TeV (from top to bottom). Error bars indicate the uncorrelated combined uncertainties, while boxes show the uncorrelated systematic uncertainties. Curves indicate predictions from PYTHIA6 (D6T and Z2 tunes) and the 4C tune of PYTHIA8.

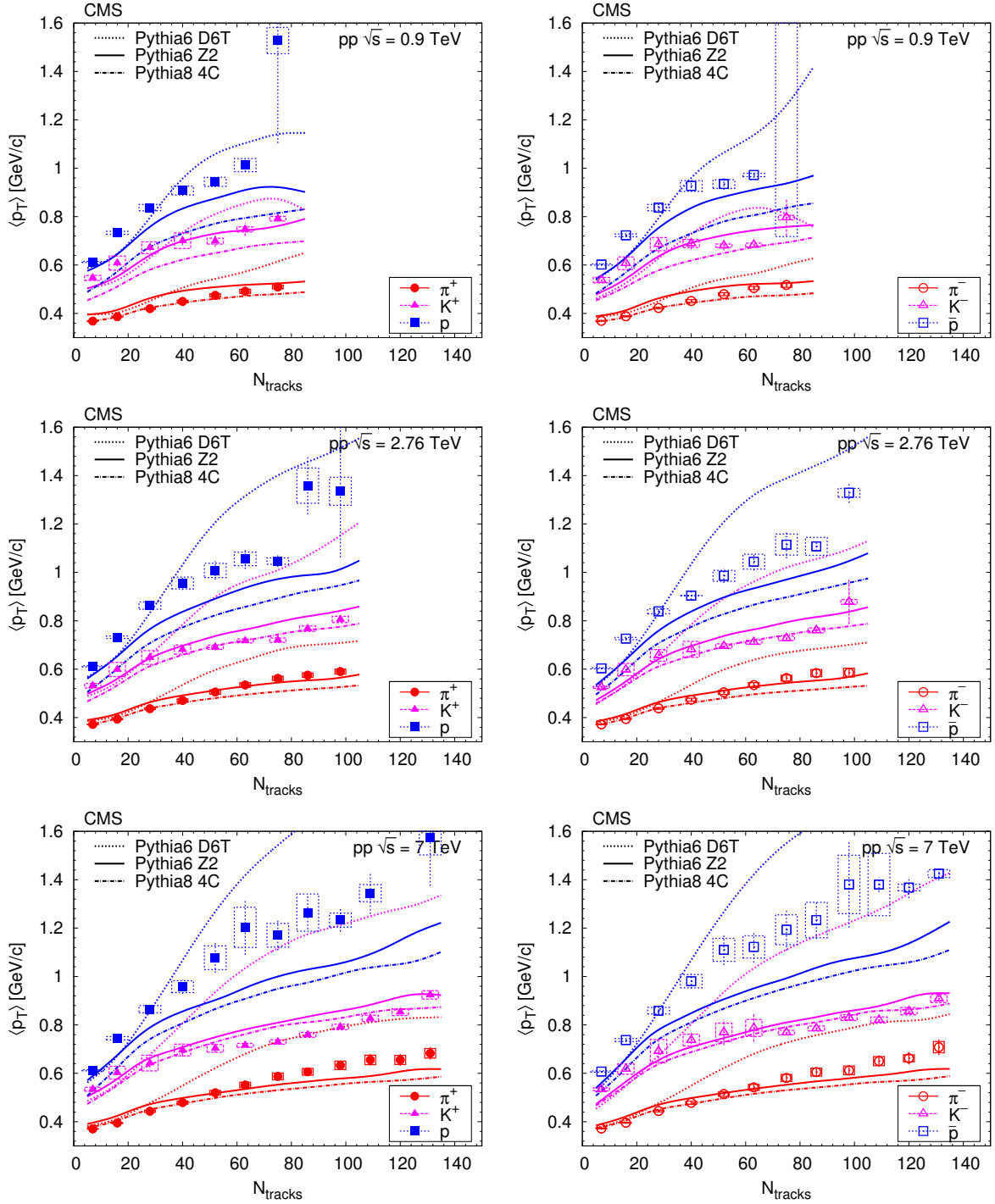


Figure 16: Average transverse momentum of identified charged hadrons (pions, kaons, protons) in the range $|y| < 1$, for positive (left) and negative (right) particles, as a function of the true track multiplicity for $|\eta| < 2.4$, at $\sqrt{s} = 0.9, 2.76$, and 7 TeV (from top to bottom). Error bars indicate the uncorrelated combined uncertainties, while boxes show the uncorrelated systematic uncertainties. The fully correlated normalisation uncertainty (not shown) is 1.0%. Curves indicate predictions from PYTHIA6 (D6T and Z2 tunes) and the 4C tune of PYTHIA8.

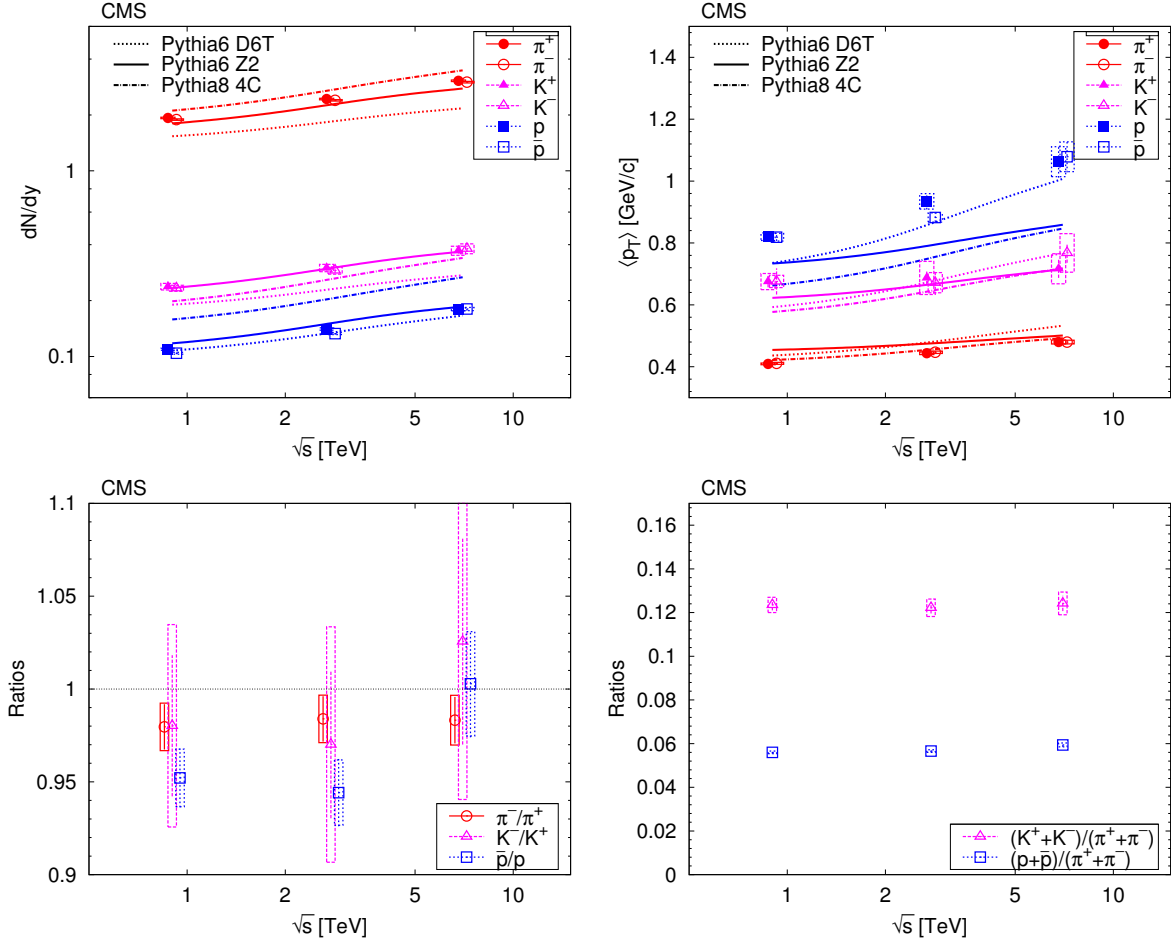


Figure 17: Center-of-mass energy dependence of dN/dy , average transverse momentum $\langle p_T \rangle$, and ratios of particle yields. Error bars indicate the uncorrelated combined uncertainties, while boxes show the uncorrelated systematic uncertainties. For dN/dy ($\langle p_T \rangle$) the fully correlated normalisation uncertainty (not shown) is 3.0% (1.0%). Curves indicate predictions from PYTHIA6 (D6T and Z2 tunes) and the 4C tune of PYTHIA8.

bian Funding Agency (COLCIENCIAS); the Croatian Ministry of Science, Education and Sport; the Research Promotion Foundation, Cyprus; the Ministry of Education and Research, Recurrent financing contract SF0690030s09 and European Regional Development Fund, Estonia; the Academy of Finland, Finnish Ministry of Education and Culture, and Helsinki Institute of Physics; the Institut National de Physique Nucléaire et de Physique des Particules / CNRS, and Commissariat à l'Énergie Atomique et aux Énergies Alternatives / CEA, France; the Bundesministerium für Bildung und Forschung, Deutsche Forschungsgemeinschaft, and Helmholtz-Gemeinschaft Deutscher Forschungszentren, Germany; the General Secretariat for Research and Technology, Greece; the National Scientific Research Foundation, and National Office for Research and Technology, Hungary; the Department of Atomic Energy and the Department of Science and Technology, India; the Institute for Studies in Theoretical Physics and Mathematics, Iran; the Science Foundation, Ireland; the Istituto Nazionale di Fisica Nucleare, Italy; the Korean Ministry of Education, Science and Technology and the World Class University program of NRF, Korea; the Lithuanian Academy of Sciences; the Mexican Funding Agencies (CINVESTAV, CONACYT, SEP, and UASLP-FAI); the Ministry of Science and Innovation, New Zealand; the Pakistan Atomic Energy Commission; the Ministry of Science and Higher Edu-

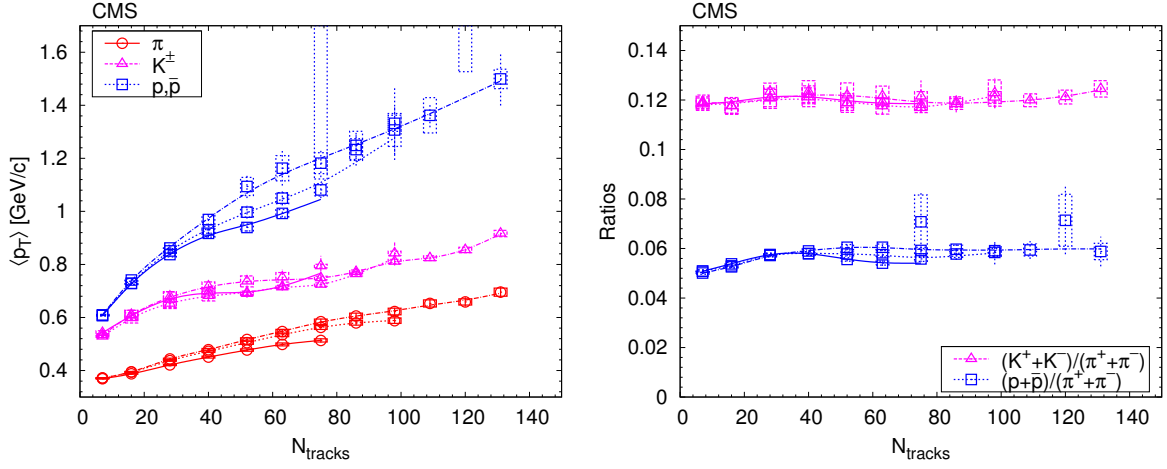


Figure 18: Left: average transverse momentum of identified charged hadrons (pions, kaons, protons) in the range $|y| < 1$, for all particle types, as a function of the true track multiplicity for $|\eta| < 2.4$, for all energies. Right: ratios of particle yields as a function of particle multiplicity for $|\eta| < 2.4$, for all energies. Error bars indicate the uncorrelated combined uncertainties, while boxes show the uncorrelated systematic uncertainties. For $\langle p_T \rangle$ the fully correlated normalisation uncertainty (not shown) is 1.0%. Lines are drawn to guide the eye (solid – 0.9 TeV, dotted – 2.76 TeV, dash-dotted – 7 TeV).

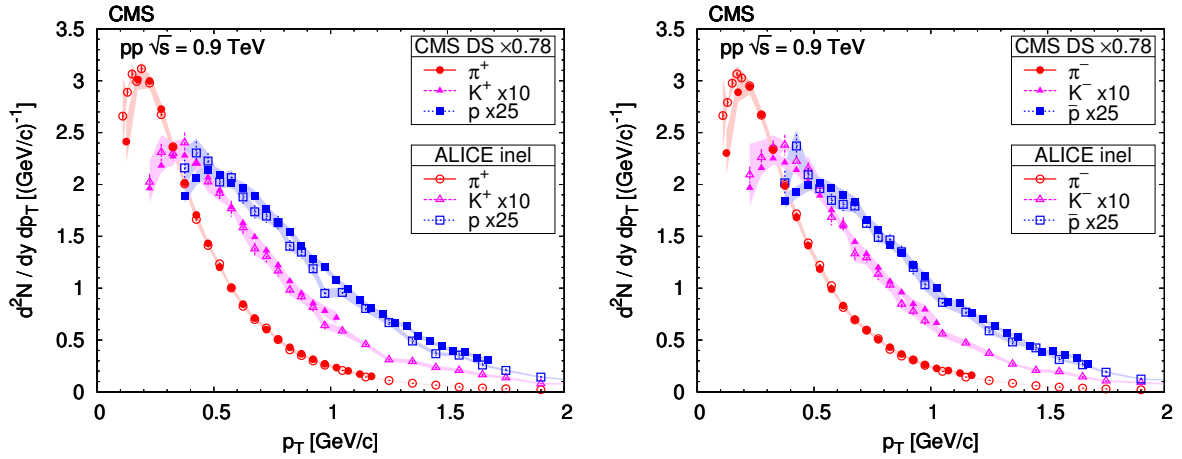


Figure 19: Comparison of transverse momentum distributions of identified charged hadrons (pions, kaons, protons) at central rapidity ($|y| < 1$ for CMS, $|y| < 0.5$ for ALICE [24]), for positive hadrons (left) and negative hadrons (right), at $\sqrt{s} = 0.9$ TeV. To improve clarity, the kaon and proton points are scaled by the quoted factors. Error bars indicate the uncorrelated statistical uncertainties, while bands show the uncorrelated systematic uncertainties. In the CMS case the fully correlated normalisation uncertainty (not shown) is 3.0%. The ALICE results were corrected to inelastic pp collisions and therefore the CMS points are scaled by an empirical factor of 0.78 so as to correct for the different particle level selection used by ALICE.

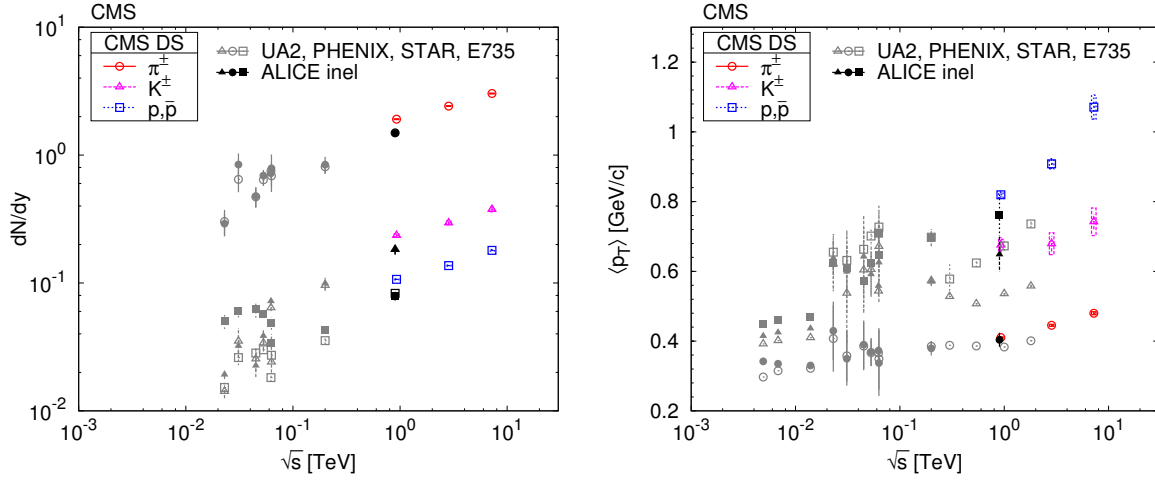


Figure 20: Comparison of the center-of-mass energy dependence of the central rapidity density dN/dy (left) and the average transverse momentum $\langle p_T \rangle$ (right). Low-energy data (UA2 [25], E735 [26], PHENIX [27], STAR [28]) are shown with LHC data (ALICE[24] and CMS). For the CMS points, the error bars indicate the uncorrelated combined uncertainties, while boxes show the uncorrelated systematic uncertainties. The fully correlated normalisation uncertainty (not shown) is around 3.0% (left plot) and 1.0% (right plot).

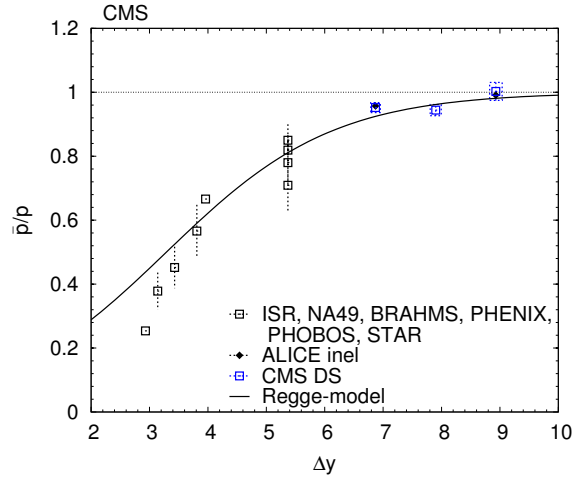


Figure 21: Comparison of the central rapidity \bar{p}/p yield ratio as a function of the rapidity difference Δy , plotted together with the prediction of the Regge-inspired model [37]. Measurements at low energies (ISR, [29, 30]), NA49 [31], BRAHMS [32], PHENIX [33], PHOBOS [34], and STAR [35] are shown along with LHC data (ALICE and CMS).

cation and the National Science Centre, Poland; the Fundação para a Ciência e a Tecnologia, Portugal; JINR (Armenia, Belarus, Georgia, Ukraine, Uzbekistan); the Ministry of Education and Science of the Russian Federation, the Federal Agency of Atomic Energy of the Russian Federation, Russian Academy of Sciences, and the Russian Foundation for Basic Research; the Ministry of Science and Technological Development of Serbia; the Secretaría de Estado de Investigación, Desarrollo e Innovación and Programa Consolider-Ingenio 2010, Spain; the Swiss Funding Agencies (ETH Board, ETH Zurich, PSI, SNF, UniZH, Canton Zurich, and SER); the National Science Council, Taipei; the Scientific and Technical Research Council of Turkey, and Turkish Atomic Energy Authority; the Science and Technology Facilities Council, UK; the US

Department of Energy, and the US National Science Foundation.

Individuals have received support from the Marie-Curie programme and the European Research Council (European Union); the Leventis Foundation; the A. P. Sloan Foundation; the Alexander von Humboldt Foundation; the Austrian Science Fund (FWF); the Belgian Federal Science Policy Office; the Fonds pour la Formation à la Recherche dans l'Industrie et dans l'Agriculture (FRIA-Belgium); the Agentschap voor Innovatie door Wetenschap en Technologie (IWT-Belgium); the Council of Science and Industrial Research, India; the Compagnia di San Paolo (Torino); and the HOMING PLUS programme of Foundation for Polish Science, co-financed from European Union, Regional Development Fund.

References

- [1] CMS Collaboration, “The CMS experiment at the CERN LHC”, *JINST* **3** (2008) S08004, doi:10.1088/1748-0221/3/08/S08004.
- [2] Particle Data Group Collaboration, “Review of particle physics”, *J. Phys. G* **37** (2010) 075021, doi:10.1088/0954-3899/37/7A/075021.
- [3] CMS Collaboration, “Commissioning and performance of the CMS pixel tracker with cosmic ray muons”, *JINST* **5** (2010) T03007, doi:10.1088/1748-0221/5/03/T03007, arXiv:0911.5434.
- [4] CMS Collaboration, “Commissioning and performance of the CMS silicon strip tracker with cosmic ray muons”, *JINST* **5** (2010) T03008, doi:10.1088/1748-0221/5/03/T03008, arXiv:0911.4996.
- [5] CMS Collaboration, “Measurement of CMS Luminosity”, CMS Physics Analysis Summary CMS-PAS-EWK-10-004, (2010).
- [6] CMS Collaboration, “Absolute luminosity normalization”, Detector Performance Summary CMS-DP-11-002, (2011).
- [7] CMS Collaboration, “Transverse momentum and pseudorapidity distributions of charged hadrons in pp collisions at $\sqrt{s} = 0.9$ and 2.36 TeV”, *JHEP* **02** (2010) 041, doi:10.1007/JHEP02(2010)041, arXiv:1002.0621.
- [8] T. Sjöstrand, S. Mrenna, and P. Z. Skands, “PYTHIA 6.4 Physics and Manual”, *JHEP* **05** (2006) 026, doi:10.1088/1126-6708/2006/05/026, arXiv:hep-ph/0603175.
- [9] R. Field, “Studying the underlying event at CDF and the LHC”, (2009). arXiv:1003.4220. Proceedings of the First International Workshop on Multiple Partonic Interactions at the LHC (MPI08).
- [10] R. Field, “Early LHC Underlying Event Data - Findings and Surprises”, (2010). arXiv:1010.3558.
- [11] F. Siklér, “Low p_T Hadronic Physics with CMS”, *Int. J. Mod. Phys. E* **16** (2007) 1819, doi:10.1142/S0218301307007052, arXiv:physics/0702193.
- [12] CMS Collaboration, “Transverse-momentum and pseudorapidity distributions of charged hadrons in pp collisions at $\sqrt{s} = 7$ TeV”, *Phys. Rev. Lett.* **105** (2010) 022002, doi:10.1103/PhysRevLett.105.022002, arXiv:1005.3299.

- [13] F. Siklér, “Study of clustering methods to improve primary vertex finding for collider detectors”, *Nucl. Instrum. Meth. A* **621** (2010) 526, doi:10.1016/j.nima.2010.04.058, arXiv:0911.2767.
- [14] CMS Collaboration, “Strange particle production in pp collisions at $\sqrt{s} = 0.9$ and 7 TeV”, *JHEP* **05** (2011) 064, doi:10.1007/JHEP05(2011)064, arXiv:1102.4282.
- [15] F. Siklér, “A parametrisation of the energy loss distributions of charged particles and its applications for silicon detectors”, *Nucl. Instrum. Meth. A* **691** (2012) 16, doi:10.1016/j.nima.2012.06.064, arXiv:1111.3213.
- [16] W. H. Press et al., “Numerical Recipes: The Art of Scientific Computing”. Cambridge University Press, Cambridge, third edition, 2007.
- [17] F. Siklér, “Particle identification with a track fit χ^2 ”, *Nucl. Instrum. Meth. A* **620** (2010) 477, doi:10.1016/j.nima.2010.03.098, arXiv:0911.2624.
- [18] R. Brun and F. Rademakers, “ROOT: An object oriented data analysis framework”, *Nucl. Instrum. Meth. A* **389** (1997) 81, doi:10.1016/S0168-9002(97)00048-X.
- [19] C. Tsallis, “Possible generalization of Boltzmann-Gibbs statistics”, *J. Stat. Phys.* **52** (1988) 479, doi:10.1007/BF01016429.
- [20] T. S. Biró, G. Purcsel, and K. Ürmösy, “Non-extensive approach to quark matter”, *Eur. Phys. J. A* **40** (2009) 325, doi:10.1140/epja/i2009-10806-6, arXiv:0812.2104.
- [21] T. Sjöstrand, S. Mrenna, and P. Z. Skands, “A Brief Introduction to PYTHIA 8.1”, *Comput. Phys. Commun.* **178** (2008) 852, doi:10.1016/j.cpc.2008.01.036, arXiv:0710.3820.
- [22] CMS Collaboration, “Observation of long-range near-side angular correlations in proton-proton collisions at the LHC”, *JHEP* **09** (2010) 091, doi:10.1007/JHEP09(2010)091, arXiv:1009.4122.
- [23] D. d’Enterria et al., “Constraints from the first LHC data on hadronic event generators for ultra-high energy cosmic-ray physics”, *Astropart. Phys.* **35** (2011) 98, doi:10.1016/j.astropartphys.2011.05.002, arXiv:1101.5596.
- [24] ALICE Collaboration, “Production of pions, kaons and protons in pp collisions at $\sqrt{s} = 900$ GeV with ALICE at the LHC”, *Eur. Phys. J. C* **71** (2011) 1, doi:10.1140/epjc/s10052-011-1655-9.
- [25] UA2 Collaboration, “Inclusive charged particle production at the CERN anti-p p collider”, *Phys. Lett. B* **122** (1983) 322, doi:10.1016/0370-2693(83)90712-8.
- [26] E735 Collaboration, “Mass-identified particle production in proton-antiproton collisions at $\sqrt{s} = 300$ GeV, 540 GeV, 1000 GeV, and 1800 GeV”, *Phys. Rev. D* **48** (1993) 984, doi:10.1103/PhysRevD.48.984.
- [27] PHENIX Collaboration, “Identified charged hadron production in $p + p$ collisions at $\sqrt{s} = 200$ and 62.4 GeV”, *Phys. Rev. C* **83** (2011) 064903, doi:10.1103/PhysRevC.83.064903, arXiv:1102.0753.
- [28] STAR Collaboration, “Strange particle production in p+p collisions at $\sqrt{s} = 200$ GeV”, *Phys. Rev. C* **75** (2007) 064901, doi:10.1103/PhysRevC.75.064901, arXiv:nucl-ex/0607033.

- [29] A. M. Rossi et al., “Experimental study of the energy dependence in proton proton inclusive reactions”, *Nucl. Phys. B* **84** (1975) 269,
doi:10.1016/0550-3213(75)90307-7.
- [30] M. Aguilar-Benitez et al., “Inclusive particle production in 400 GeV/c pp interactions”, *Z. Phys. C* **50** (1991) 405, doi:10.1007/BF01551452.
- [31] NA49 Collaboration, “Inclusive production of protons, anti-protons and neutrons in p+p collisions at 158 GeV/c beam momentum”, *Eur. Phys. J. C* **65** (2010) 9,
doi:10.1140/epjc/s10052-009-1172-2, arXiv:0904.2708.
- [32] BRAHMS Collaboration, “Forward and midrapidity like-particle ratios from p + p collisions at $\sqrt{s} = 200$ GeV”, *Phys. Lett. B* **607** (2005) 42,
doi:10.1016/j.physletb.2004.12.064, arXiv:nucl-ex/0409002.
- [33] PHENIX Collaboration, “Identified charged particle spectra and yields in Au+Au collisions at $\sqrt{s_{NN}} = 200$ GeV”, *Phys. Rev. C* **69** (2004) 034909,
doi:10.1103/PhysRevC.69.034909, arXiv:nucl-ex/0307022.
- [34] PHOBOS Collaboration, “Charged antiparticle to particle ratios near midrapidity in p + p collisions at $\sqrt{s_{NN}} = 200$ GeV”, *Phys. Rev. C* **71** (2005) 021901,
doi:10.1103/PhysRevC.71.021901, arXiv:nucl-ex/0409003.
- [35] STAR Collaboration, “Systematic measurements of identified particle spectra in pp, d+Au and Au+Au Collisions at the STAR detector”, *Phys. Rev. C* **79** (2009) 034909,
doi:10.1103/PhysRevC.79.034909, arXiv:0808.2041.
- [36] ALICE Collaboration, “Midrapidity antiproton-to-proton ratio in pp collisions at $\sqrt{s} = 0.9$ and 7 TeV measured by the ALICE experiment”, *Phys. Rev. Lett.* **105** (2010) 072002,
doi:10.1103/PhysRevLett.105.072002, arXiv:1006.5432.
- [37] D. Kharzeev, “Can gluons trace baryon number?”, *Phys. Lett. B* **378** (1996) 238,
doi:10.1016/0370-2693(96)00435-2, arXiv:nucl-th/9602027.
- [38] LHCb Collaboration, “Measurement of prompt hadron production ratios in pp collisions at $\sqrt{s} = 0.9$ and 7 TeV”, (2012). arXiv:1206.5160. Submitted to Eur. Phys. J. C.

A The CMS Collaboration

Yerevan Physics Institute, Yerevan, Armenia

S. Chatrchyan, V. Khachatryan, A.M. Sirunyan, A. Tumasyan

Institut für Hochenergiephysik der OeAW, Wien, Austria

W. Adam, E. Aguilo, T. Bergauer, M. Dragicevic, J. Erö, C. Fabjan¹, M. Friedl, R. Frühwirth¹, V.M. Ghete, J. Hammer, N. Hörmann, J. Hrubec, M. Jeitler¹, W. Kiesenhofer, V. Knünz, M. Krammer¹, I. Krätschmer, D. Liko, I. Mikulec, M. Pernicka[†], B. Rahbaran, C. Rohringer, H. Rohringer, R. Schöfbeck, J. Strauss, A. Taurok, W. Waltenberger, G. Walzel, E. Widl, C.-E. Wulz¹

National Centre for Particle and High Energy Physics, Minsk, Belarus

V. Mossolov, N. Shumeiko, J. Suarez Gonzalez

Universiteit Antwerpen, Antwerpen, Belgium

S. Bansal, T. Cornelis, E.A. De Wolf, X. Janssen, S. Luyckx, L. Mucibello, S. Ochesanu, B. Roland, R. Rougny, M. Selvaggi, Z. Staykova, H. Van Haevermaet, P. Van Mechelen, N. Van Remortel, A. Van Spilbeeck

Vrije Universiteit Brussel, Brussel, Belgium

F. Blekman, S. Blyweert, J. D'Hondt, R. Gonzalez Suarez, A. Kalogeropoulos, M. Maes, A. Olbrechts, W. Van Doninck, P. Van Mulders, G.P. Van Onsem, I. Villella

Université Libre de Bruxelles, Bruxelles, Belgium

B. Clerbaux, G. De Lentdecker, V. Dero, A.P.R. Gay, T. Hreus, A. Léonard, P.E. Marage, T. Reis, L. Thomas, G. Vander Marcken, C. Vander Velde, P. Vanlaer, J. Wang

Ghent University, Ghent, Belgium

V. Adler, K. Beernaert, A. Cimmino, S. Costantini, G. Garcia, M. Grunewald, B. Klein, J. Lellouch, A. Marinov, J. McCartin, A.A. Ocampo Rios, D. Ryckbosch, N. Strobbe, F. Thyssen, M. Tytgat, P. Verwilligen, S. Walsh, E. Yazgan, N. Zaganidis

Université Catholique de Louvain, Louvain-la-Neuve, Belgium

S. Basegmez, G. Bruno, R. Castello, L. Ceard, C. Delaere, T. du Pree, D. Favart, L. Forthomme, A. Giammanco², J. Hollar, V. Lemaitre, J. Liao, O. Militaru, C. Nuttens, D. Pagano, A. Pin, K. Piotrkowski, N. Schul, J.M. Vizan Garcia

Université de Mons, Mons, Belgium

N. Beliy, T. Caebergs, E. Daubie, G.H. Hammad

Centro Brasileiro de Pesquisas Fisicas, Rio de Janeiro, Brazil

G.A. Alves, M. Correa Martins Junior, D. De Jesus Damiao, T. Martins, M.E. Pol, M.H.G. Souza

Universidade do Estado do Rio de Janeiro, Rio de Janeiro, Brazil

W.L. Aldá Júnior, W. Carvalho, A. Custódio, E.M. Da Costa, C. De Oliveira Martins, S. Fonseca De Souza, D. Matos Figueiredo, L. Mundim, H. Nogima, V. Oguri, W.L. Prado Da Silva, A. Santoro, L. Soares Jorge, A. Sznajder

Instituto de Fisica Teorica, Universidade Estadual Paulista, Sao Paulo, Brazil

T.S. Anjos³, C.A. Bernardes³, F.A. Dias⁴, T.R. Fernandez Perez Tomei, E. M. Gregores³, C. Lagana, F. Marinho, P.G. Mercadante³, S.F. Novaes, Sandra S. Padula

Institute for Nuclear Research and Nuclear Energy, Sofia, Bulgaria

V. Genchev⁵, P. Iaydjiev⁵, S. Piperov, M. Rodozov, S. Stoykova, G. Sultanov, V. Tcholakov, R. Trayanov, M. Vutova

University of Sofia, Sofia, Bulgaria

A. Dimitrov, R. Hadjiiska, V. Kozhuharov, L. Litov, B. Pavlov, P. Petkov

Institute of High Energy Physics, Beijing, China

J.G. Bian, G.M. Chen, H.S. Chen, C.H. Jiang, D. Liang, S. Liang, X. Meng, J. Tao, J. Wang, X. Wang, Z. Wang, H. Xiao, M. Xu, J. Zang, Z. Zhang

State Key Lab. of Nucl. Phys. and Tech., Peking University, Beijing, China

C. Asawatangtrakuldee, Y. Ban, S. Guo, Y. Guo, W. Li, S. Liu, Y. Mao, S.J. Qian, H. Teng, D. Wang, L. Zhang, B. Zhu, W. Zou

Universidad de Los Andes, Bogota, Colombia

C. Avila, J.P. Gomez, B. Gomez Moreno, A.F. Osorio Oliveros, J.C. Sanabria

Technical University of Split, Split, Croatia

N. Godinovic, D. Lelas, R. Plestina⁶, D. Polic, I. Puljak⁵

University of Split, Split, Croatia

Z. Antunovic, M. Kovac

Institute Rudjer Boskovic, Zagreb, Croatia

V. Brigljevic, S. Duric, K. Kadija, J. Luetic, S. Morovic

University of Cyprus, Nicosia, Cyprus

A. Attikis, M. Galanti, G. Mavromanolakis, J. Mousa, C. Nicolaou, F. Ptochos, P.A. Razis

Charles University, Prague, Czech Republic

M. Finger, M. Finger Jr.

Academy of Scientific Research and Technology of the Arab Republic of Egypt, Egyptian Network of High Energy Physics, Cairo, Egypt

Y. Assran⁷, S. Elgammal⁸, A. Ellithi Kamel⁹, S. Khalil⁸, M.A. Mahmoud¹⁰, A. Radi^{11,12}

National Institute of Chemical Physics and Biophysics, Tallinn, Estonia

M. Kadastik, M. Müntel, M. Raidal, L. Rebane, A. Tiko

Department of Physics, University of Helsinki, Helsinki, Finland

P. Eerola, G. Fedi, M. Voutilainen

Helsinki Institute of Physics, Helsinki, Finland

J. Härkönen, A. Heikkinen, V. Karimäki, R. Kinnunen, M.J. Kortelainen, T. Lampén, K. Lassila-Perini, S. Lehti, T. Lindén, P. Luukka, T. Mäenpää, T. Peltola, E. Tuominen, J. Tuominiemi, E. Tuovinen, D. Ungaro, L. Wendland

Lappeenranta University of Technology, Lappeenranta, Finland

K. Banzuzi, A. Karjalainen, A. Korpela, T. Tuuva

DSM/IRFU, CEA/Saclay, Gif-sur-Yvette, France

M. Besancon, S. Choudhury, M. Dejardin, D. Denegri, B. Fabbro, J.L. Faure, F. Ferri, S. Ganjour, A. Givernaud, P. Gras, G. Hamel de Monchenault, P. Jarry, E. Locci, J. Malcles, L. Millischer, A. Nayak, J. Rander, A. Rosowsky, I. Shreyber, M. Titov

Laboratoire Leprince-Ringuet, Ecole Polytechnique, IN2P3-CNRS, Palaiseau, France

S. Baffioni, F. Beaudette, L. Benhabib, L. Bianchini, M. Bluj¹³, C. Broutin, P. Busson, C. Charlot, N. Daci, T. Dahms, L. Dobrzynski, R. Granier de Cassagnac, M. Haguenaue, P. Miné, C. Mironov, I.N. Naranjo, M. Nguyen, C. Ochando, P. Paganini, D. Sabes, R. Salerno, Y. Sirois, C. Veelken, A. Zabi

Institut Pluridisciplinaire Hubert Curien, Université de Strasbourg, Université de Haute Alsace Mulhouse, CNRS/IN2P3, Strasbourg, France

J.-L. Agram¹⁴, J. Andrea, D. Bloch, D. Bodin, J.-M. Brom, M. Cardaci, E.C. Chabert, C. Collard, E. Conte¹⁴, F. Drouhin¹⁴, C. Ferro, J.-C. Fontaine¹⁴, D. Gelé, U. Goerlach, P. Juillot, A.-C. Le Bihan, P. Van Hove

Centre de Calcul de l'Institut National de Physique Nucleaire et de Physique des Particules (IN2P3), Villeurbanne, France

F. Fassi, D. Mercier

Université de Lyon, Université Claude Bernard Lyon 1, CNRS-IN2P3, Institut de Physique Nucléaire de Lyon, Villeurbanne, France

S. Beauceron, N. Beaupere, O. Bondu, G. Boudoul, J. Chasserat, R. Chierici⁵, D. Contardo, P. Depasse, H. El Mamouni, J. Fay, S. Gascon, M. Gouzevitch, B. Ille, T. Kurca, M. Lethuillier, L. Mirabito, S. Perries, V. Sordini, Y. Tschudi, P. Verdier, S. Viret

E. Andronikashvili Institute of Physics, Academy of Science, Tbilisi, Georgia

V. Roinishvili

RWTH Aachen University, I. Physikalisches Institut, Aachen, Germany

G. Anagnostou, S. Beranek, M. Edelhoff, L. Feld, N. Heracleous, O. Hindrichs, R. Jussen, K. Klein, J. Merz, A. Ostapchuk, A. Perieanu, F. Raupach, J. Sammet, S. Schael, D. Sprenger, H. Weber, B. Wittmer, V. Zhukov¹⁵

RWTH Aachen University, III. Physikalisches Institut A, Aachen, Germany

M. Ata, J. Caudron, E. Dietz-Laursonn, D. Duchardt, M. Erdmann, R. Fischer, A. Güth, T. Hebbeker, C. Heidemann, K. Hoepfner, D. Klingebiel, P. Kreuzer, C. Magass, M. Merschmeyer, A. Meyer, M. Olschewski, P. Papacz, H. Pieta, H. Reithler, S.A. Schmitz, L. Sonnenschein, J. Steggemann, D. Teyssier, M. Weber

RWTH Aachen University, III. Physikalisches Institut B, Aachen, Germany

M. Bontenackels, V. Cherepanov, G. Flüge, H. Geenen, M. Geisler, W. Haj Ahmad, F. Hoehle, B. Kargoll, T. Kress, Y. Kuessel, A. Nowack, L. Perchalla, O. Pooth, P. Sauerland, A. Stahl

Deutsches Elektronen-Synchrotron, Hamburg, Germany

M. Aldaya Martin, J. Behr, W. Behrenhoff, U. Behrens, M. Bergholz¹⁶, A. Bethani, K. Borrás, A. Burgmeier, A. Cakir, L. Calligaris, A. Campbell, E. Castro, F. Costanza, D. Dammann, C. Diez Pardos, G. Eckerlin, D. Eckstein, G. Flucke, A. Geiser, I. Glushkov, P. Gunnellini, S. Habib, J. Hauk, G. Hellwig, H. Jung, M. Kasemann, P. Katsas, C. Kleinwort, H. Kluge, A. Knutsson, M. Krämer, D. Krücker, E. Kuznetsova, W. Lange, W. Lohmann¹⁶, B. Lutz, R. Mankel, I. Marfin, M. Marienfeld, I.-A. Melzer-Pellmann, A.B. Meyer, J. Mnich, A. Mussgiller, S. Naumann-Emme, J. Olzem, H. Perrey, A. Petrukhin, D. Pitzl, A. Raspereza, P.M. Ribeiro Cipriano, C. Riedl, E. Ron, M. Rosin, J. Salfeld-Nebgen, R. Schmidt¹⁶, T. Schoerner-Sadenius, N. Sen, A. Spiridonov, M. Stein, R. Walsh, C. Wissing

University of Hamburg, Hamburg, Germany

C. Autermann, V. Blobel, J. Draeger, H. Enderle, J. Erfle, U. Gebbert, M. Görner, T. Hermanns, R.S. Høing, K. Kaschube, G. Kaussen, H. Kirschenmann, R. Klanner, J. Lange, B. Mura, F. Nowak, T. Peiffer, N. Pietsch, D. Rathjens, C. Sander, H. Schettler, P. Schleper, E. Schlieckau, A. Schmidt, M. Schröder, T. Schum, M. Seidel, V. Sola, H. Stadie, G. Steinbrück, J. Thomsen, L. Vanelderen

Institut für Experimentelle Kernphysik, Karlsruhe, Germany

C. Barth, J. Berger, C. Böser, T. Chwalek, W. De Boer, A. Descroix, A. Dierlamm, M. Feindt,

M. Guthoff⁵, C. Hackstein, F. Hartmann, T. Hauth⁵, M. Heinrich, H. Held, K.H. Hoffmann, S. Honc, I. Katkov¹⁵, J.R. Komaragiri, P. Lobelle Pardo, D. Martschei, S. Mueller, Th. Müller, M. Niegel, A. Nürnberg, O. Oberst, A. Oehler, J. Ott, G. Quast, K. Rabbertz, F. Ratnikov, N. Ratnikova, S. Röcker, A. Scheurer, F.-P. Schilling, G. Schott, H.J. Simonis, F.M. Stober, D. Troendle, R. Ulrich, J. Wagner-Kuhr, S. Wayand, T. Weiler, M. Zeise

Institute of Nuclear Physics "Demokritos", Aghia Paraskevi, Greece

G. Daskalakis, T. Geralis, S. Kesisoglou, A. Kyriakis, D. Loukas, I. Manolakos, A. Markou, C. Markou, C. Mavrommatis, E. Ntomari

University of Athens, Athens, Greece

L. Gouskos, T.J. Mertzimekis, A. Panagiotou, N. Saoulidou

University of Ioánnina, Ioánnina, Greece

I. Evangelou, C. Foudas⁵, P. Kokkas, N. Manthos, I. Papadopoulos, V. Patras

KFKI Research Institute for Particle and Nuclear Physics, Budapest, Hungary

G. Bencze, C. Hajdu⁵, P. Hidas, D. Horvath¹⁷, F. Sikler, V. Veszpremi, G. Vesztergombi¹⁸

Institute of Nuclear Research ATOMKI, Debrecen, Hungary

N. Beni, S. Czellar, J. Molnar, J. Palinkas, Z. Szillasi

University of Debrecen, Debrecen, Hungary

J. Karancsi, P. Raics, Z.L. Trocsanyi, B. Ujvari

Panjab University, Chandigarh, India

S.B. Beri, V. Bhatnagar, N. Dhingra, R. Gupta, M. Jindal, M. Kaur, M.Z. Mehta, N. Nishu, L.K. Saini, A. Sharma, J. Singh

University of Delhi, Delhi, India

Ashok Kumar, Arun Kumar, S. Ahuja, A. Bhardwaj, B.C. Choudhary, S. Malhotra, M. Naimuddin, K. Ranjan, V. Sharma, R.K. Shivpuri

Saha Institute of Nuclear Physics, Kolkata, India

S. Banerjee, S. Bhattacharya, S. Dutta, B. Gomber, Sa. Jain, Sh. Jain, R. Khurana, S. Sarkar, M. Sharan

Bhabha Atomic Research Centre, Mumbai, India

A. Abdulsalam, R.K. Choudhury, D. Dutta, S. Kailas, V. Kumar, P. Mehta, A.K. Mohanty⁵, L.M. Pant, P. Shukla

Tata Institute of Fundamental Research - EHEP, Mumbai, India

T. Aziz, S. Ganguly, M. Guchait¹⁹, M. Maity²⁰, G. Majumder, K. Mazumdar, G.B. Mohanty, B. Parida, K. Sudhakar, N. Wickramage

Tata Institute of Fundamental Research - HECR, Mumbai, India

S. Banerjee, S. Dugad

Institute for Research in Fundamental Sciences (IPM), Tehran, Iran

H. Arfaei, H. Bakhshiansohi²¹, S.M. Etesami²², A. Fahim²¹, M. Hashemi, H. Hesari, A. Jafari²¹, M. Khakzad, M. Mohammadi Najafabadi, S. Paktinat Mehdiabadi, B. Safarzadeh²³, M. Zeinali²²

INFN Sezione di Bari ^a, Università di Bari ^b, Politecnico di Bari ^c, Bari, Italy

M. Abbrescia^{a,b}, L. Barbone^{a,b}, C. Calabria^{a,b,5}, S.S. Chhibra^{a,b}, A. Colaleo^a, D. Creanza^{a,c}, N. De Filippis^{a,c,5}, M. De Palma^{a,b}, L. Fiore^a, G. Iaselli^{a,c}, L. Lusito^{a,b}, G. Maggi^{a,c},

M. Maggi^a, B. Marangelli^{a,b}, S. My^{a,c}, S. Nuzzo^{a,b}, N. Pacifico^{a,b}, A. Pompili^{a,b}, G. Pugliese^{a,c}, G. Selvaggi^{a,b}, L. Silvestris^a, G. Singh^{a,b}, R. Venditti, G. Zito^a

INFN Sezione di Bologna ^a, Università di Bologna ^b, Bologna, Italy

G. Abbiendi^a, A.C. Benvenuti^a, D. Bonacorsi^{a,b}, S. Braibant-Giacomelli^{a,b}, L. Brigliadori^{a,b}, P. Capiluppi^{a,b}, A. Castro^{a,b}, F.R. Cavallo^a, M. Cuffiani^{a,b}, G.M. Dallavalle^a, F. Fabbri^a, A. Fanfani^{a,b}, D. Fasanella^{a,b,5}, P. Giacomelli^a, C. Grandi^a, L. Guiducci^{a,b}, S. Marcellini^a, G. Masetti^a, M. Meneghelli^{a,b,5}, A. Montanari^a, F.L. Navarria^{a,b}, F. Odorici^a, A. Perrotta^a, F. Primavera^{a,b}, A.M. Rossi^{a,b}, T. Rovelli^{a,b}, G. Siroli^{a,b}, R. Travaglini^{a,b}

INFN Sezione di Catania ^a, Università di Catania ^b, Catania, Italy

S. Albergo^{a,b}, G. Cappello^{a,b}, M. Chiorboli^{a,b}, S. Costa^{a,b}, R. Potenza^{a,b}, A. Tricomi^{a,b}, C. Tuve^{a,b}

INFN Sezione di Firenze ^a, Università di Firenze ^b, Firenze, Italy

G. Barbagli^a, V. Ciulli^{a,b}, C. Civinini^a, R. D'Alessandro^{a,b}, E. Focardi^{a,b}, S. Frosali^{a,b}, E. Gallo^a, S. Gonzi^{a,b}, M. Meschini^a, S. Paoletti^a, G. Sguazzoni^a, A. Tropiano^{a,5}

INFN Laboratori Nazionali di Frascati, Frascati, Italy

L. Benussi, S. Bianco, S. Colafranceschi²⁴, F. Fabbri, D. Piccolo

INFN Sezione di Genova, Genova, Italy

P. Fabbriatore, R. Musenich, S. Tosi

INFN Sezione di Milano-Bicocca ^a, Università di Milano-Bicocca ^b, Milano, Italy

A. Benaglia^{a,b,5}, F. De Guio^{a,b}, L. Di Matteo^{a,b,5}, S. Fiorendi^{a,b}, S. Gennai^{a,5}, A. Ghezzi^{a,b}, S. Malvezzi^a, R.A. Manzoni^{a,b}, A. Martelli^{a,b}, A. Massironi^{a,b,5}, D. Menasce^a, L. Moroni^a, M. Paganoni^{a,b}, D. Pedrini^a, S. Ragazzi^{a,b}, N. Redaelli^a, S. Sala^a, T. Tabarelli de Fatis^{a,b}

INFN Sezione di Napoli ^a, Università di Napoli "Federico II" ^b, Napoli, Italy

S. Buontempo^a, C.A. Carrillo Montoya^a, N. Cavallo^{a,25}, A. De Cosa^{a,b,5}, O. Dogangun^{a,b}, F. Fabozzi^{a,25}, A.O.M. Iorio^a, L. Lista^a, S. Meola^{a,26}, M. Merola^{a,b}, P. Paolucci^{a,5}

INFN Sezione di Padova ^a, Università di Padova ^b, Università di Trento (Trento) ^c, Padova, Italy

P. Azzi^a, N. Bacchetta^{a,5}, D. Bisello^{a,b}, A. Branca^{a,b,5}, R. Carlin^{a,b}, P. Checchia^a, T. Dorigo^a, F. Gasparini^{a,b}, F. Gonella^a, A. Gozzelino^a, K. Kanishchev^{a,c}, S. Lacaprara^a, I. Lazzizzera^{a,c}, M. Margoni^{a,b}, A.T. Meneguzzo^{a,b}, M. Passaseo^a, J. Pazzini^{a,b}, N. Pozzobon^{a,b}, P. Ronchese^{a,b}, F. Simonetto^{a,b}, E. Torassa^a, M. Tosi^{a,b,5}, S. Vanini^{a,b}, P. Zotto^{a,b}, G. Zumerle^{a,b}

INFN Sezione di Pavia ^a, Università di Pavia ^b, Pavia, Italy

M. Gabusi^{a,b}, S.P. Ratti^{a,b}, C. Riccardi^{a,b}, P. Torre^{a,b}, P. Vitulo^{a,b}

INFN Sezione di Perugia ^a, Università di Perugia ^b, Perugia, Italy

M. Biasini^{a,b}, G.M. Bilei^a, L. Fanò^{a,b}, P. Lariccia^{a,b}, A. Lucaroni^{a,b,5}, G. Mantovani^{a,b}, M. Menichelli^a, A. Nappi^{a,b}, F. Romeo^{a,b}, A. Saha^a, A. Santocchia^{a,b}, A. Spiezia^{a,b}, S. Taroni^{a,b,5}

INFN Sezione di Pisa ^a, Università di Pisa ^b, Scuola Normale Superiore di Pisa ^c, Pisa, Italy

P. Azzurri^{a,c}, G. Bagliesi^a, T. Boccali^a, G. Broccolo^{a,c}, R. Castaldi^a, R.T. D'Agnolo^{a,c}, R. Dell'Orso^a, F. Fiori^{a,b,5}, L. Foà^{a,c}, A. Giassi^a, A. Kraan^a, F. Ligabue^{a,c}, T. Lomtadze^a, L. Martini^{a,27}, A. Messineo^{a,b}, F. Palla^a, A. Rizzi^{a,b}, A.T. Serban^{a,28}, P. Spagnolo^a, P. Squillacioti^{a,5}, R. Tenchini^a, G. Tonelli^{a,b,5}, A. Venturi^{a,5}, P.G. Verdini^a

INFN Sezione di Roma ^a, Università di Roma "La Sapienza" ^b, Roma, Italy

L. Barone^{a,b}, F. Cavallari^a, D. Del Re^{a,b,5}, M. Diemoz^a, C. Fanelli, M. Grassi^{a,b,5}, E. Longo^{a,b}

P. Meridiani^{a,5}, F. Micheli^{a,b}, S. Nourbakhsh^{a,b}, G. Organtini^{a,b}, R. Paramatti^a, S. Rahatlou^{a,b}, M. Sigamani^a, L. Soffi^{a,b}

INFN Sezione di Torino ^a, Università di Torino ^b, Università del Piemonte Orientale (Novara) ^c, Torino, Italy

N. Amapane^{a,b}, R. Arcidiacono^{a,c}, S. Argiro^{a,b}, M. Arneodo^{a,c}, C. Biino^a, N. Cartiglia^a, M. Costa^{a,b}, N. Demaria^a, C. Mariotti^{a,5}, S. Maselli^a, E. Migliore^{a,b}, V. Monaco^{a,b}, M. Musich^{a,5}, M.M. Obertino^{a,c}, N. Pastrone^a, M. Pelliccioni^a, A. Potenza^{a,b}, A. Romero^{a,b}, M. Ruspa^{a,c}, R. Sacchi^{a,b}, A. Solano^{a,b}, A. Staiano^a, A. Vilela Pereira^a

INFN Sezione di Trieste ^a, Università di Trieste ^b, Trieste, Italy

S. Belforte^a, V. Candelise^{a,b}, F. Cossutti^a, G. Della Ricca^{a,b}, B. Gobbo^a, M. Marone^{a,b,5}, D. Montanino^{a,b,5}, A. Penzo^a, A. Schizzi^{a,b}

Kangwon National University, Chunchon, Korea

S.G. Heo, T.Y. Kim, S.K. Nam

Kyungpook National University, Daegu, Korea

S. Chang, D.H. Kim, G.N. Kim, D.J. Kong, H. Park, S.R. Ro, D.C. Son, T. Son

Chonnam National University, Institute for Universe and Elementary Particles, Kwangju, Korea

J.Y. Kim, Zero J. Kim, S. Song

Korea University, Seoul, Korea

S. Choi, D. Gyun, B. Hong, M. Jo, H. Kim, T.J. Kim, K.S. Lee, D.H. Moon, S.K. Park

University of Seoul, Seoul, Korea

M. Choi, J.H. Kim, C. Park, I.C. Park, S. Park, G. Ryu

Sungkyunkwan University, Suwon, Korea

Y. Cho, Y. Choi, Y.K. Choi, J. Goh, M.S. Kim, E. Kwon, B. Lee, J. Lee, S. Lee, H. Seo, I. Yu

Vilnius University, Vilnius, Lithuania

M.J. Bilinskas, I. Grigelionis, M. Janulis, A. Juodagalvis

Centro de Investigacion y de Estudios Avanzados del IPN, Mexico City, Mexico

H. Castilla-Valdez, E. De La Cruz-Burelo, I. Heredia-de La Cruz, R. Lopez-Fernandez, R. Magaña Villalba, J. Martínez-Ortega, A. Sánchez-Hernández, L.M. Villasenor-Cendejas

Universidad Iberoamericana, Mexico City, Mexico

S. Carrillo Moreno, F. Vazquez Valencia

Benemerita Universidad Autonoma de Puebla, Puebla, Mexico

H.A. Salazar Ibarguen

Universidad Autónoma de San Luis Potosí, San Luis Potosí, Mexico

E. Casimiro Linares, A. Morelos Pineda, M.A. Reyes-Santos

University of Auckland, Auckland, New Zealand

D. Krofcheck

University of Canterbury, Christchurch, New Zealand

A.J. Bell, P.H. Butler, R. Doesburg, S. Reucroft, H. Silverwood

National Centre for Physics, Quaid-I-Azam University, Islamabad, Pakistan

M. Ahmad, M.H. Ansari, M.I. Asghar, H.R. Hoorani, S. Khalid, W.A. Khan, T. Khurshid, S. Qazi, M.A. Shah, M. Shoaib

Institute of Experimental Physics, Faculty of Physics, University of Warsaw, Warsaw, Poland

G. Brona, K. Bunkowski, M. Cwiok, W. Dominik, K. Doroba, A. Kalinowski, M. Konecki, J. Krolikowski

Soltan Institute for Nuclear Studies, Warsaw, Poland

H. Bialkowska, B. Boimska, T. Frueboes, R. Gokieli, M. Górski, M. Kazana, K. Nawrocki, K. Romanowska-Rybinska, M. Szleper, G. Wrochna, P. Zalewski

Laboratório de Instrumentação e Física Experimental de Partículas, Lisboa, Portugal

N. Almeida, P. Bargassa, A. David, P. Faccioli, P.G. Ferreira Parracho, M. Gallinaro, J. Seixas, J. Varela, P. Vischia

Joint Institute for Nuclear Research, Dubna, Russia

I. Belotelov, P. Bunin, M. Gavrilenko, I. Golutvin, I. Gorbunov, A. Kamenev, V. Karjavin, G. Kozlov, A. Lanev, A. Malakhov, P. Moisenz, V. Palichik, V. Perelygin, S. Shmatov, V. Smirnov, A. Volodko, A. Zarubin

Petersburg Nuclear Physics Institute, Gatchina (St Petersburg), Russia

S. Evstyukhin, V. Golovtsov, Y. Ivanov, V. Kim, P. Levchenko, V. Murzin, V. Oreshkin, I. Smirnov, V. Sulimov, L. Uvarov, S. Vavilov, A. Vorobyev, An. Vorobyev

Institute for Nuclear Research, Moscow, Russia

Yu. Andreev, A. Dermenev, S. Gninenko, N. Golubev, M. Kirsanov, N. Krasnikov, V. Matveev, A. Pashenkov, D. Tlisov, A. Toropin

Institute for Theoretical and Experimental Physics, Moscow, Russia

V. Epshteyn, M. Erofeeva, V. Gavrilov, M. Kossov⁵, N. Lychkovskaya, V. Popov, G. Safronov, S. Semenov, V. Stolin, E. Vlasov, A. Zhokin

Moscow State University, Moscow, Russia

A. Belyaev, E. Boos, M. Dubinin⁴, L. Dudko, L. Khein, V. Klyukhin, O. Kodolova, I. Lokhtin, A. Markina, S. Obraztsov, M. Perfilov, S. Petrushanko, A. Popov, A. Proskuryakov, L. Sarycheva[†], V. Savrin, A. Snigirev

P.N. Lebedev Physical Institute, Moscow, Russia

V. Andreev, M. Azarkin, I. Dremin, M. Kirakosyan, A. Leonidov, G. Mesyats, S.V. Rusakov, A. Vinogradov

State Research Center of Russian Federation, Institute for High Energy Physics, Protvino, Russia

I. Azhgirey, I. Bayshev, S. Bitioukov, V. Grishin⁵, V. Kachanov, D. Konstantinov, A. Korablev, V. Krychkine, V. Petrov, R. Ryutin, A. Sobol, L. Tourtchanovitch, S. Troshin, N. Tyurin, A. Uzunian, A. Volkov

University of Belgrade, Faculty of Physics and Vinca Institute of Nuclear Sciences, Belgrade, Serbia

P. Adzic²⁹, M. Djordjevic, M. Ekmedzic, D. Krpic²⁹, J. Milosevic

Centro de Investigaciones Energéticas Medioambientales y Tecnológicas (CIEMAT), Madrid, Spain

M. Aguilar-Benitez, J. Alcaraz Maestre, P. Arce, C. Battilana, E. Calvo, M. Cerrada, M. Chamizo

Llatas, N. Colino, B. De La Cruz, A. Delgado Peris, D. Domínguez Vázquez, C. Fernandez Bedoya, J.P. Fernández Ramos, A. Ferrando, J. Flix, M.C. Fouz, P. Garcia-Abia, O. Gonzalez Lopez, S. Goy Lopez, J.M. Hernandez, M.I. Josa, G. Merino, J. Puerta Pelayo, A. Quintario Olmeda, I. Redondo, L. Romero, J. Santaolalla, M.S. Soares, C. Willmott

Universidad Autónoma de Madrid, Madrid, Spain

C. Albajar, G. Codispoti, J.F. de Trocóniz

Universidad de Oviedo, Oviedo, Spain

H. Brun, J. Cuevas, J. Fernandez Menendez, S. Folgueras, I. Gonzalez Caballero, L. Lloret Iglesias, J. Piedra Gomez³⁰

Instituto de Física de Cantabria (IFCA), CSIC-Universidad de Cantabria, Santander, Spain

J.A. Brochero Cifuentes, I.J. Cabrillo, A. Calderon, S.H. Chuang, J. Duarte Campderros, M. Felcini³¹, M. Fernandez, G. Gomez, J. Gonzalez Sanchez, A. Graziano, C. Jorda, A. Lopez Virto, J. Marco, R. Marco, C. Martinez Rivero, F. Matorras, F.J. Munoz Sanchez, T. Rodrigo, A.Y. Rodríguez-Marrero, A. Ruiz-Jimeno, L. Scodellaro, M. Sobron Sanudo, I. Vila, R. Vilar Cortabitarte

CERN, European Organization for Nuclear Research, Geneva, Switzerland

D. Abbaneo, E. Auffray, G. Auzinger, P. Baillon, A.H. Ball, D. Barney, J.F. Benitez, C. Bernet⁶, G. Bianchi, P. Bloch, A. Bocci, A. Bonato, C. Botta, H. Breuker, T. Camporesi, G. Cerminara, T. Christiansen, J.A. Coarasa Perez, D. D'Enterria, A. Dabrowski, A. De Roeck, S. Di Guida, M. Dobson, N. Dupont-Sagorin, A. Elliott-Peisert, B. Frisch, W. Funk, G. Georgiou, M. Giffels, D. Gigi, K. Gill, D. Giordano, M. Giunta, F. Glege, R. Gomez-Reino Garrido, P. Govoni, S. Gowdy, R. Guida, M. Hansen, P. Harris, C. Hartl, J. Harvey, B. Hegner, A. Hinzmann, V. Innocente, P. Janot, K. Kaadze, E. Karavakis, K. Kousouris, P. Lecoq, Y.-J. Lee, P. Lenzi, C. Lourenço, T. Mäki, M. Malberti, L. Malgeri, M. Mannelli, L. Masetti, F. Meijers, S. Mersi, E. Meschi, R. Moser, M.U. Mozer, M. Mulders, P. Musella, E. Nesvold, T. Orimoto, L. Orsini, E. Palencia Cortezon, E. Perez, L. Perrozzi, A. Petrilli, A. Pfeiffer, M. Pierini, M. Pimiä, D. Piparo, G. Polese, L. Quertenmont, A. Racz, W. Reece, J. Rodrigues Antunes, G. Rolandi³², C. Rovelli³³, M. Rovere, H. Sakulin, F. Santanastasio, C. Schäfer, C. Schwick, I. Segoni, S. Sekmen, A. Sharma, P. Siegrist, P. Silva, M. Simon, P. Sphicas³⁴, D. Spiga, A. Tsiros, G.I. Veres¹⁸, J.R. Vlimant, H.K. Wöhri, S.D. Worm³⁵, W.D. Zeuner

Paul Scherrer Institut, Villigen, Switzerland

W. Bertl, K. Deiters, W. Erdmann, K. Gabathuler, R. Horisberger, Q. Ingram, H.C. Kaestli, S. König, D. Kotlinski, U. Langenegger, F. Meier, D. Renker, T. Rohe, J. Sibille³⁶

Institute for Particle Physics, ETH Zurich, Zurich, Switzerland

L. Bäni, P. Bortignon, M.A. Buchmann, B. Casal, N. Chanon, A. Deisher, G. Dissertori, M. Dittmar, M. Donegà, M. Dünser, J. Eugster, K. Freudenreich, C. Grab, D. Hits, P. Lecomte, W. Lustermann, A.C. Marini, P. Martinez Ruiz del Arbol, N. Mohr, F. Moortgat, C. Nägeli³⁷, P. Nef, F. Nessi-Tedaldi, F. Pandolfi, L. Pape, F. Pauss, M. Peruzzi, F.J. Ronga, M. Rossini, L. Sala, A.K. Sanchez, A. Starodumov³⁸, B. Stieger, M. Takahashi, L. Tauscher[†], A. Thea, K. Theofilatos, D. Treille, C. Urscheler, R. Wallny, H.A. Weber, L. Wehrli

Universität Zürich, Zurich, Switzerland

C. Amsler, V. Chiochia, S. De Visscher, C. Favaro, M. Ivova Rikova, B. Millan Mejias, P. Otiougova, P. Robmann, H. Snoek, S. Tupputi, M. Verzetti

National Central University, Chung-Li, Taiwan

Y.H. Chang, K.H. Chen, C.M. Kuo, S.W. Li, W. Lin, Z.K. Liu, Y.J. Lu, D. Mekterovic, A.P. Singh, R. Volpe, S.S. Yu

National Taiwan University (NTU), Taipei, Taiwan

P. Bartalini, P. Chang, Y.H. Chang, Y.W. Chang, Y. Chao, K.F. Chen, C. Dietz, U. Grundler, W.-S. Hou, Y. Hsiung, K.Y. Kao, Y.J. Lei, R.-S. Lu, D. Majumder, E. Petrakou, X. Shi, J.G. Shiu, Y.M. Tzeng, X. Wan, M. Wang

Cukurova University, Adana, Turkey

A. Adiguzel, M.N. Bakirci³⁹, S. Cerci⁴⁰, C. Dozen, I. Dumanoglu, E. Eskut, S. Girgis, G. Gokbulut, E. Gurpinar, I. Hos, E.E. Kangal, T. Karaman, G. Karapinar⁴¹, A. Kayis Topaksu, G. Onengut, K. Ozdemir, S. Ozturk⁴², A. Polatoz, K. Sogut⁴³, D. Sunar Cerci⁴⁰, B. Tali⁴⁰, H. Topakli³⁹, L.N. Vergili, M. Vergili

Middle East Technical University, Physics Department, Ankara, Turkey

I.V. Akin, T. Aliev, B. Bilin, S. Bilmis, M. Deniz, H. Gamsizkan, A.M. Guler, K. Ocalan, A. Ozpineci, M. Serin, R. Sever, U.E. Surat, M. Yalvac, E. Yildirim, M. Zeyrek

Bogazici University, Istanbul, Turkey

E. Gülmez, B. Isildak⁴⁴, M. Kaya⁴⁵, O. Kaya⁴⁵, S. Ozkorucuklu⁴⁶, N. Sonmez⁴⁷

Istanbul Technical University, Istanbul, Turkey

K. Cankocak

National Scientific Center, Kharkov Institute of Physics and Technology, Kharkov, Ukraine

L. Levchuk

University of Bristol, Bristol, United Kingdom

F. Bostock, J.J. Brooke, E. Clement, D. Cussans, H. Flacher, R. Frazier, J. Goldstein, M. Grimes, G.P. Heath, H.F. Heath, L. Kreczko, S. Metson, D.M. Newbold³⁵, K. Nirunpong, A. Poll, S. Senkin, V.J. Smith, T. Williams

Rutherford Appleton Laboratory, Didcot, United Kingdom

L. Basso⁴⁸, K.W. Bell, A. Belyaev⁴⁸, C. Brew, R.M. Brown, D.J.A. Cockerill, J.A. Coughlan, K. Harder, S. Harper, J. Jackson, B.W. Kennedy, E. Olaiya, D. Petyt, B.C. Radburn-Smith, C.H. Shepherd-Themistocleous, I.R. Tomalin, W.J. Womersley

Imperial College, London, United Kingdom

R. Bainbridge, G. Ball, R. Beuselinck, O. Buchmuller, D. Colling, N. Cripps, M. Cutajar, P. Dauncey, G. Davies, M. Della Negra, W. Ferguson, J. Fulcher, D. Futyan, A. Gilbert, A. Guneratne Bryer, G. Hall, Z. Hatherell, J. Hays, G. Iles, M. Jarvis, G. Karapostoli, L. Lyons, A.-M. Magnan, J. Marrouche, B. Mathias, R. Nandi, J. Nash, A. Nikitenko³⁸, A. Papageorgiou, J. Pela⁵, M. Pesaresi, K. Petridis, M. Pioppi⁴⁹, D.M. Raymond, S. Rogerson, A. Rose, M.J. Ryan, C. Seez, P. Sharp[†], A. Sparrow, M. Stoye, A. Tapper, M. Vazquez Acosta, T. Virdee, S. Wakefield, N. Wardle, T. Whyntie

Brunel University, Uxbridge, United Kingdom

M. Chadwick, J.E. Cole, P.R. Hobson, A. Khan, P. Kyberd, D. Leggat, D. Leslie, W. Martin, I.D. Reid, P. Symonds, L. Teodorescu, M. Turner

Baylor University, Waco, USA

K. Hatakeyama, H. Liu, T. Scarborough

The University of Alabama, Tuscaloosa, USA

O. Charaf, C. Henderson, P. Rumerio

Boston University, Boston, USA

A. Avetisyan, T. Bose, C. Fantasia, A. Heister, J. St. John, P. Lawson, D. Lazic, J. Rohlf, D. Sperka, L. Sulak

Brown University, Providence, USA

J. Alimena, S. Bhattacharya, D. Cutts, A. Ferapontov, U. Heintz, S. Jabeen, G. Kukartsev, E. Laird, G. Landsberg, M. Luk, M. Narain, D. Nguyen, M. Segala, T. Sinthuprasith, T. Speer, K.V. Tsang

University of California, Davis, Davis, USA

R. Breedon, G. Breto, M. Calderon De La Barca Sanchez, S. Chauhan, M. Chertok, J. Conway, R. Conway, P.T. Cox, J. Dolen, R. Erbacher, M. Gardner, R. Houtz, W. Ko, A. Kopecky, R. Lander, T. Miceli, D. Pellett, F. Ricci-tam, B. Rutherford, M. Searle, J. Smith, M. Squires, M. Tripathi, R. Vasquez Sierra

University of California, Los Angeles, Los Angeles, USA

V. Andreev, D. Cline, R. Cousins, J. Duris, S. Erhan, P. Everaerts, C. Farrell, J. Hauser, M. Ignatenko, C. Jarvis, C. Plager, G. Rakness, P. Schlein[†], P. Traczyk, V. Valuev, M. Weber

University of California, Riverside, Riverside, USA

J. Babb, R. Clare, M.E. Dinardo, J. Ellison, J.W. Gary, F. Giordano, G. Hanson, G.Y. Jeng⁵⁰, H. Liu, O.R. Long, A. Luthra, H. Nguyen, S. Paramesvaran, J. Sturdy, S. Sumowidagdo, R. Wilken, S. Wimpenny

University of California, San Diego, La Jolla, USA

W. Andrews, J.G. Branson, G.B. Cerati, S. Cittolin, D. Evans, F. Golf, A. Holzner, R. Kelley, M. Lebourgeois, J. Letts, I. Macneill, B. Mangano, S. Padhi, C. Palmer, G. Petrucciani, M. Pieri, M. Sani, V. Sharma, S. Simon, E. Sudano, M. Tadel, Y. Tu, A. Vartak, S. Wasserbaech⁵¹, F. Würthwein, A. Yagil, J. Yoo

University of California, Santa Barbara, Santa Barbara, USA

D. Barge, R. Bellan, C. Campagnari, M. D'Alfonso, T. Danielson, K. Flowers, P. Geffert, J. Incandela, C. Justus, P. Kalavase, S.A. Koay, D. Kovalskyi, V. Krutelyov, S. Lowette, N. Mccoll, V. Pavlunin, F. Rebassoo, J. Ribnik, J. Richman, R. Rossin, D. Stuart, W. To, C. West

California Institute of Technology, Pasadena, USA

A. Apresyan, A. Bornheim, Y. Chen, E. Di Marco, J. Duarte, M. Gataullin, Y. Ma, A. Mott, H.B. Newman, C. Rogan, M. Spiropulu⁴, V. Timciuc, J. Veverka, R. Wilkinson, Y. Yang, R.Y. Zhu

Carnegie Mellon University, Pittsburgh, USA

B. Akgun, V. Azzolini, R. Carroll, T. Ferguson, Y. Iiyama, D.W. Jang, Y.F. Liu, M. Paulini, H. Vogel, I. Vorobiev

University of Colorado at Boulder, Boulder, USA

J.P. Cumalat, B.R. Drell, C.J. Edelmaier, W.T. Ford, A. Gaz, B. Heyburn, E. Luigi Lopez, J.G. Smith, K. Stenson, K.A. Ulmer, S.R. Wagner

Cornell University, Ithaca, USA

J. Alexander, A. Chatterjee, N. Eggert, L.K. Gibbons, B. Heltsley, A. Khukhunaishvili, B. Kreis, N. Mirman, G. Nicolas Kaufman, J.R. Patterson, A. Ryd, E. Salvati, W. Sun, W.D. Teo, J. Thom, J. Thompson, J. Tucker, J. Vaughan, Y. Weng, L. Winstrom, P. Wittich

Fairfield University, Fairfield, USA

D. Winn

Fermi National Accelerator Laboratory, Batavia, USA

S. Abdullin, M. Albrow, J. Anderson, L.A.T. Bauerdick, A. Beretvas, J. Berryhill, P.C. Bhat, I. Bloch, K. Burkett, J.N. Butler, V. Chetluru, H.W.K. Cheung, F. Chlebana, V.D. Elvira, I. Fisk, J. Freeman, Y. Gao, D. Green, O. Gutsche, J. Hanlon, R.M. Harris, J. Hirschauer, B. Hooberman, S. Jindariani, M. Johnson, U. Joshi, B. Kilminster, B. Klima, S. Kunori, S. Kwan, C. Leonidopoulos, J. Linacre, D. Lincoln, R. Lipton, J. Lykken, K. Maeshima, J.M. Marraffino, S. Maruyama, D. Mason, P. McBride, K. Mishra, S. Mrenna, Y. Musienko⁵², C. Newman-Holmes, V. O'Dell, O. Prokofyev, E. Sexton-Kennedy, S. Sharma, W.J. Spalding, L. Spiegel, P. Tan, L. Taylor, S. Tkaczyk, N.V. Tran, L. Uplegger, E.W. Vaandering, R. Vidal, J. Whitmore, W. Wu, F. Yang, F. Yumiceva, J.C. Yun

University of Florida, Gainesville, USA

D. Acosta, P. Avery, D. Bourilkov, M. Chen, T. Cheng, S. Das, M. De Gruttola, G.P. Di Giovanni, D. Dobur, A. Drozdetskiy, R.D. Field, M. Fisher, Y. Fu, I.K. Furic, J. Gartner, J. Hugon, B. Kim, J. Konigsberg, A. Korytov, A. Kropivnitskaya, T. Kypreos, J.F. Low, K. Matchev, P. Milenovic⁵³, G. Mitselmakher, L. Muniz, R. Remington, A. Rinkevicius, P. Sellers, N. Skhirtladze, M. Snowball, J. Yelton, M. Zakaria

Florida International University, Miami, USA

V. Gaultney, S. Hewamanage, L.M. Lebolo, S. Linn, P. Markowitz, G. Martinez, J.L. Rodriguez

Florida State University, Tallahassee, USA

T. Adams, A. Askew, J. Bochenek, J. Chen, B. Diamond, S.V. Gleyzer, J. Haas, S. Hagopian, V. Hagopian, M. Jenkins, K.F. Johnson, H. Prosper, V. Veeraraghavan, M. Weinberg

Florida Institute of Technology, Melbourne, USA

M.M. Baarmand, B. Dorney, M. Hohlmann, H. Kalakhety, I. Vodopiyanov

University of Illinois at Chicago (UIC), Chicago, USA

M.R. Adams, I.M. Anghel, L. Apanasevich, Y. Bai, V.E. Bazterra, R.R. Betts, I. Bucinskaite, J. Callner, R. Cavanaugh, C. Dragoiu, O. Evdokimov, L. Gauthier, C.E. Gerber, D.J. Hofman, S. Khalatyan, F. Lacroix, M. Malek, C. O'Brien, C. Silkworth, D. Strom, N. Varelas

The University of Iowa, Iowa City, USA

U. Akgun, E.A. Albayrak, B. Bilki⁵⁴, W. Clarida, F. Duru, S. Griffiths, J.-P. Merlo, H. Mermerkaya⁵⁵, A. Mestvirishvili, A. Moeller, J. Nachtman, C.R. Newsom, E. Norbeck, Y. Onel, F. Ozok, S. Sen, E. Tiras, J. Wetzel, T. Yetkin, K. Yi

Johns Hopkins University, Baltimore, USA

B.A. Barnett, B. Blumenfeld, S. Bolognesi, D. Fehling, G. Giurgiu, A.V. Gritsan, Z.J. Guo, G. Hu, P. Maksimovic, S. Rappoccio, M. Swartz, A. Whitbeck

The University of Kansas, Lawrence, USA

P. Baringer, A. Bean, G. Benelli, O. Grachov, R.P. Kenny Iii, M. Murray, D. Noonan, S. Sanders, R. Stringer, G. Tinti, J.S. Wood, V. Zhukova

Kansas State University, Manhattan, USA

A.F. Barfuss, T. Bolton, I. Chakaberia, A. Ivanov, S. Khalil, M. Makouski, Y. Maravin, S. Shrestha, I. Svintradze

Lawrence Livermore National Laboratory, Livermore, USA

J. Gronberg, D. Lange, D. Wright

University of Maryland, College Park, USA

A. Baden, M. Boutemeur, B. Calvert, S.C. Eno, J.A. Gomez, N.J. Hadley, R.G. Kellogg, M. Kirn,

T. Kolberg, Y. Lu, M. Marionneau, A.C. Mignerey, K. Pedro, A. Peterman, A. Skuja, J. Temple, M.B. Tonjes, S.C. Tonwar, E. Twedt

Massachusetts Institute of Technology, Cambridge, USA

A. Apyan, G. Bauer, J. Bendavid, W. Busza, E. Butz, I.A. Cali, M. Chan, V. Dutta, G. Gomez Ceballos, M. Goncharov, K.A. Hahn, Y. Kim, M. Klute, K. Krajczar⁵⁶, W. Li, P.D. Luckey, T. Ma, S. Nahn, C. Paus, D. Ralph, C. Roland, G. Roland, M. Rudolph, G.S.F. Stephans, F. Stöckli, K. Sumorok, K. Sung, D. Velicanu, E.A. Wenger, R. Wolf, B. Wyslouch, S. Xie, M. Yang, Y. Yilmaz, A.S. Yoon, M. Zanetti

University of Minnesota, Minneapolis, USA

S.I. Cooper, B. Dahmes, A. De Benedetti, G. Franzoni, A. Gude, S.C. Kao, K. Klapoetke, Y. Kubota, J. Mans, N. Pastika, R. Rusack, M. Sasseville, A. Singovsky, N. Tambe, J. Turkewitz

University of Mississippi, University, USA

L.M. Cremaldi, R. Kroeger, L. Perera, R. Rahmat, D.A. Sanders

University of Nebraska-Lincoln, Lincoln, USA

E. Avdeeva, K. Bloom, S. Bose, J. Butt, D.R. Claes, A. Dominguez, M. Eads, J. Keller, I. Kravchenko, J. Lazo-Flores, H. Malbouisson, S. Malik, G.R. Snow

State University of New York at Buffalo, Buffalo, USA

U. Baur, A. Godshalk, I. Iashvili, S. Jain, A. Kharchilava, A. Kumar, S.P. Shipkowski, K. Smith

Northeastern University, Boston, USA

G. Alverson, E. Barberis, D. Baumgartel, M. Chasco, J. Haley, D. Nash, D. Trocino, D. Wood, J. Zhang

Northwestern University, Evanston, USA

A. Anastassov, A. Kubik, N. Mucia, N. Odell, R.A. Ofierzynski, B. Pollack, A. Pozdnyakov, M. Schmitt, S. Stoynev, M. Velasco, S. Won

University of Notre Dame, Notre Dame, USA

L. Antonelli, D. Berry, A. Brinkerhoff, M. Hildreth, C. Jessop, D.J. Karmgard, J. Kolb, K. Lannon, W. Luo, S. Lynch, N. Marinelli, D.M. Morse, T. Pearson, R. Ruchti, J. Slaunwhite, N. Valls, M. Wayne, M. Wolf

The Ohio State University, Columbus, USA

B. Bylsma, L.S. Durkin, C. Hill, R. Hughes, K. Kotov, T.Y. Ling, D. Puigh, M. Rodenburg, C. Vuosalo, G. Williams, B.L. Winer

Princeton University, Princeton, USA

N. Adam, E. Berry, P. Elmer, D. Gerbaudo, V. Halyo, P. Hebda, J. Hegeman, A. Hunt, P. Jindal, D. Lopes Pegna, P. Lujan, D. Marlow, T. Medvedeva, M. Mooney, J. Olsen, P. Piroué, X. Quan, A. Raval, B. Safdi, H. Saka, D. Stickland, C. Tully, J.S. Werner, A. Zuranski

University of Puerto Rico, Mayaguez, USA

J.G. Acosta, E. Brownson, X.T. Huang, A. Lopez, H. Mendez, S. Oliveros, J.E. Ramirez Vargas, A. Zatserklyaniy

Purdue University, West Lafayette, USA

E. Alagoz, V.E. Barnes, D. Benedetti, G. Bolla, D. Bortoletto, M. De Mattia, A. Everett, Z. Hu, M. Jones, O. Koybasi, M. Kress, A.T. Laasanen, N. Leonardo, V. Maroussov, P. Merkel, D.H. Miller, N. Neumeister, I. Shipsey, D. Silvers, A. Svyatkovskiy, M. Vidal Marono, H.D. Yoo, J. Zablocki, Y. Zheng

Purdue University Calumet, Hammond, USA

S. Guragain, N. Parashar

Rice University, Houston, USA

A. Adair, C. Boulahouache, K.M. Ecklund, F.J.M. Geurts, B.P. Padley, R. Redjimi, J. Roberts, J. Zabel

University of Rochester, Rochester, USA

B. Betchart, A. Bodek, Y.S. Chung, R. Covarelli, P. de Barbaro, R. Demina, Y. Eshaq, A. Garcia-Bellido, P. Goldenzweig, J. Han, A. Harel, D.C. Miner, D. Vishnevskiy, M. Zielinski

The Rockefeller University, New York, USA

A. Bhatti, R. Ciesielski, L. Demortier, K. Goulios, G. Lungu, S. Malik, C. Mesropian

Rutgers, the State University of New Jersey, Piscataway, USA

S. Arora, A. Barker, J.P. Chou, C. Contreras-Campana, E. Contreras-Campana, D. Duggan, D. Ferencek, Y. Gershtein, R. Gray, E. Halkiadakis, D. Hidas, A. Lath, S. Panwalkar, M. Park, R. Patel, V. Rekovic, J. Robles, K. Rose, S. Salur, S. Schnetzer, C. Seitz, S. Somalwar, R. Stone, S. Thomas

University of Tennessee, Knoxville, USA

G. Cerizza, M. Hollingsworth, S. Spanier, Z.C. Yang, A. York

Texas A&M University, College Station, USA

R. Eusebi, W. Flanagan, J. Gilmore, T. Kamon⁵⁷, V. Khotilovich, R. Montalvo, I. Osipenkov, Y. Pakhotin, A. Perloff, J. Roe, A. Safonov, T. Sakuma, S. Sengupta, I. Suarez, A. Tatarinov, D. Toback

Texas Tech University, Lubbock, USA

N. Akchurin, J. Damgov, P.R. Duderod, C. Jeong, K. Kovitanggoon, S.W. Lee, T. Libeiro, Y. Roh, I. Volobouev

Vanderbilt University, Nashville, USA

E. Appelt, A.G. Delannoy, C. Florez, S. Greene, A. Gurrola, W. Johns, C. Johnston, P. Kurt, C. Maguire, A. Melo, M. Sharma, P. Sheldon, B. Snook, S. Tuo, J. Velkovska

University of Virginia, Charlottesville, USA

M.W. Arenton, M. Balazs, S. Boutle, B. Cox, B. Francis, J. Goodell, R. Hirosky, A. Ledovskoy, C. Lin, C. Neu, J. Wood, R. Yohay

Wayne State University, Detroit, USA

S. Gollapinni, R. Harr, P.E. Karchin, C. Kottachchi Kankanamge Don, P. Lamichhane, A. Sakharov

University of Wisconsin, Madison, USA

M. Anderson, M. Bachtis, D. Belknap, L. Borrello, D. Carlsmith, M. Cepeda, S. Dasu, L. Gray, K.S. Grogg, M. Grothe, R. Hall-Wilton, M. Herndon, A. Hervé, P. Klabbers, J. Klukas, A. Lanaro, C. Lazaridis, J. Leonard, R. Loveless, A. Mohapatra, I. Ojalvo, F. Palmonari, G.A. Pierro, I. Ross, A. Savin, W.H. Smith, J. Swanson

†: Deceased

1: Also at Vienna University of Technology, Vienna, Austria

2: Also at National Institute of Chemical Physics and Biophysics, Tallinn, Estonia

3: Also at Universidade Federal do ABC, Santo Andre, Brazil

4: Also at California Institute of Technology, Pasadena, USA

- 5: Also at CERN, European Organization for Nuclear Research, Geneva, Switzerland
- 6: Also at Laboratoire Leprince-Ringuet, Ecole Polytechnique, IN2P3-CNRS, Palaiseau, France
- 7: Also at Suez Canal University, Suez, Egypt
- 8: Also at Zewail City of Science and Technology, Zewail, Egypt
- 9: Also at Cairo University, Cairo, Egypt
- 10: Also at Fayoum University, El-Fayoum, Egypt
- 11: Also at British University, Cairo, Egypt
- 12: Now at Ain Shams University, Cairo, Egypt
- 13: Also at Soltan Institute for Nuclear Studies, Warsaw, Poland
- 14: Also at Université de Haute-Alsace, Mulhouse, France
- 15: Also at Moscow State University, Moscow, Russia
- 16: Also at Brandenburg University of Technology, Cottbus, Germany
- 17: Also at Institute of Nuclear Research ATOMKI, Debrecen, Hungary
- 18: Also at Eötvös Loránd University, Budapest, Hungary
- 19: Also at Tata Institute of Fundamental Research - HECR, Mumbai, India
- 20: Also at University of Visva-Bharati, Santiniketan, India
- 21: Also at Sharif University of Technology, Tehran, Iran
- 22: Also at Isfahan University of Technology, Isfahan, Iran
- 23: Also at Plasma Physics Research Center, Science and Research Branch, Islamic Azad University, Teheran, Iran
- 24: Also at Facoltà Ingegneria Università di Roma, Roma, Italy
- 25: Also at Università della Basilicata, Potenza, Italy
- 26: Also at Università degli Studi Guglielmo Marconi, Roma, Italy
- 27: Also at Università degli studi di Siena, Siena, Italy
- 28: Also at University of Bucharest, Faculty of Physics, Bucuresti-Magurele, Romania
- 29: Also at Faculty of Physics of University of Belgrade, Belgrade, Serbia
- 30: Also at University of Florida, Gainesville, USA
- 31: Also at University of California, Los Angeles, Los Angeles, USA
- 32: Also at Scuola Normale e Sezione dell' INFN, Pisa, Italy
- 33: Also at INFN Sezione di Roma; Università di Roma "La Sapienza", Roma, Italy
- 34: Also at University of Athens, Athens, Greece
- 35: Also at Rutherford Appleton Laboratory, Didcot, United Kingdom
- 36: Also at The University of Kansas, Lawrence, USA
- 37: Also at Paul Scherrer Institut, Villigen, Switzerland
- 38: Also at Institute for Theoretical and Experimental Physics, Moscow, Russia
- 39: Also at Gaziosmanpasa University, Tokat, Turkey
- 40: Also at Adiyaman University, Adiyaman, Turkey
- 41: Also at Izmir Institute of Technology, Izmir, Turkey
- 42: Also at The University of Iowa, Iowa City, USA
- 43: Also at Mersin University, Mersin, Turkey
- 44: Also at Ozyegin University, Istanbul, Turkey
- 45: Also at Kafkas University, Kars, Turkey
- 46: Also at Suleyman Demirel University, Isparta, Turkey
- 47: Also at Ege University, Izmir, Turkey
- 48: Also at School of Physics and Astronomy, University of Southampton, Southampton, United Kingdom
- 49: Also at INFN Sezione di Perugia; Università di Perugia, Perugia, Italy
- 50: Also at University of Sydney, Sydney, Australia
- 51: Also at Utah Valley University, Orem, USA

52: Also at Institute for Nuclear Research, Moscow, Russia

53: Also at University of Belgrade, Faculty of Physics and Vinca Institute of Nuclear Sciences, Belgrade, Serbia

54: Also at Argonne National Laboratory, Argonne, USA

55: Also at Erzincan University, Erzincan, Turkey

56: Also at KFKI Research Institute for Particle and Nuclear Physics, Budapest, Hungary

57: Also at Kyungpook National University, Daegu, Korea